A Spatially Integrated Dissolved Inorganic Carbon (SiDIC) Model for Aquatic Ecosystems Considering Submerged Vegetation

Nagatomo, K. ; Nakayama, K. ; Komai, K. ; Matsumoto, H. ; Watanabe, K. ; Kubo, A. ; Tada, K. ; Maruya, Y. ; Yano, S. ; Tsai, J. W. ; Lin, H.…

(Citation)
Journal of Geophysical Research: Biogeosciences,128(2):e2022JG007032

(Issue Date)
2023-02

(Resource Type)
journal article

(Version)
Version of Record

(URL)
https://hdl.handle.net/20.500.14094/0100479411

JGR Biogeosciences

RESEARCH ARTICLE
10.1029/2022JG007032

Key Points:

- Submerged vegetation promotes stratification in shallow freshwater and coastal lakes which can impact net CO_2 capture
- Model results demonstrate that vegetation properties mediate the diurnal pCO_2 excursion by influencing vertical exchange with the canopy
- The results highlight the importance of resolving vegetation-mediated changes in mixing when estimating carbon uptake by submerged canopies

Correspondence to:
K. Nakayama,
nakayama@phoenix.kobe-u.ac.jp

Citation:
Nagatomo, K., Nakayama, K., Komai, K., Matsumoto, H., Watanabe, K., Kubo, A., et al. (2023). A spatially integrated dissolved inorganic carbon (SiDIC) model for aquatic ecosystems considering submerged vegetation. *Journal of Geophysical Research: Biogeosciences*, *128*, e2022JG007032. https://doi.org/10.1029/2022JG007032

Received 7 JUN 2022
Accepted 23 JAN 2023

A Spatially Integrated Dissolved Inorganic Carbon (SiDIC) Model for Aquatic Ecosystems Considering Submerged Vegetation

K. Nagatomo[1], K. Nakayama[1], K. Komai[2], H. Matsumoto[3], K. Watanabe[4], A. Kubo[5], K. Tada[6], Y. Maruya[7], S. Yano[7], J. W. Tsai[8], H. C. Lin[9], M. Vilas[10], and M. R. Hipsey[11]

[1]Graduate School of Engineering, Kobe University, Kobe City, Japan, [2]School of Earth, Energy and Environmental Engineering, Kitami Institute of Technology, Kitami, Japan, [3]Marine Pollution Management Group, Marine Environment Control System Department, Port and Airport Research Institute, Yokosuka, Japan, [4]Coastal and Estuarine Environment Research Group, Port and Airport Research Institute, Yokosuka, Japan, [5]Department of Geoscience, Shizuoka University, Suruga-ku, Japan, [6]River Sabo and Ports Department, Oriental Consultants Co., Ltd., Osaka, Japan, [7]Graduate School of Engineering, Kyushu University, Fukuoka, Japan, [8]Graduate Institute of Bioresources, National Pingtung University of Science and Technology, Neipu, Taiwan, [9]Department of Geography, National Taiwan University, Taipei City, Taiwan, [10]Department of Environment and Science, Queensland Government, Warwick, Australia, [11]Centre for Water and Spatial Science, UWA School of Agriculture and Environment, The University of Western Australia, Perth, Australia

Abstract Net ecosystem production (NEP) by submerged aquatic vegetation plays a substantial role in capturing atmospheric carbon dioxide into aquatic ecosystems. In lakes and estuaries, the net uptake of carbon dioxide by submerged aquatic vegetation is mediated by stratification of the water column which suppresses the vertical flux of carbon dioxide between the upper and lower layers. The presence of submerged aquatic vegetation can also affect the strength of stratification such that the interactions between vegetation, stratification, and NEP can moderate the carbon dioxide emissions. Since stratification can occur in lakes and estuaries, there is need for a new numerical approach able to consider the effect of submerged aquatic vegetation on stratification, NEP, and carbon dioxide. This study aims to develop a model to investigate how stratification, mediated by vegetation density and flexibility, affects the partial pressure of carbon dioxide (pCO_2) and dissolved inorganic carbon (DIC). After initial parameterization of coefficients based on experimental work, horizontal and vertical variations in DIC were successfully modeled by a spatially (horizontally) integrated DIC (SiDIC) model, which was validated with field observations from an estuarine and freshwater lake case study. The SiDIC model was able to reproduce the pCO_2 changes between daytime and nighttime throughout the water column. Sensitivity tests showed that the fluctuation of pCO_2 was controlled by the suppression of stratification due to the density of submerged aquatic vegetation. The results highlight the importance of resolving vegetation-induced stratification when modeling the carbon budget within freshwater lakes and coastal environments.

Plain Language Summary The key idea of the present study is that "vegetation-induced stratification" suppresses vertical mixing in lakes and plays a substantial role in determining how much atmospheric carbon dioxide exchanges with the water. Field observations in Komuke Lagoon and Lake Monger were used to create a representative data set for understanding dissolved inorganic carbon (DIC) metabolism in coastal and freshwater lake ecosystems, respectively. A spatially integrated DIC model was then created to reveal that the fluctuation of partial pressure of carbon dioxide was controlled by the suppression of stratification which is related to the density of submerged aquatic vegetation. The results demonstrate the effect of submerged aquatic vegetation on the vertical mixing of DIC, with implications for our understanding of carbon capture within aquatic ecosystems.

1. Introduction

Extreme weather events and natural disasters have occurred worldwide due to global warming, underscoring the urgent necessity of climate change mitigation (IPCC, 2014, 2018, 2021). Nellemann et al. (2009) have shown that much of the Earth's carbon is captured and stored naturally as "blue carbon" in oceanic and coastal ecosystems, with vegetated habitats, such as mangroves and submerged aquatic vegetation (SAV), accounting for more than 50% of all carbon storage in ocean sediment. Previous studies have shown that SAV enhances the stratification

of the water column (Nakayama, Sato, et al., 2020), suppressing vertical water exchange in shallow water areas (Ghisalberti & Nepf, 2006, 2009). When stratification occurs, large amounts of dissolved inorganic carbon (DIC) can accumulate in the deeper layers of an aquatic ecosystem because the dampening of vertical mixing prevents the flux of carbon between the upper and lower layers (Lin et al., 2021, 2022). Therefore, by suppressing vertical water exchange, SAV presence can limit the supply of carbon dioxide from bottom waters to the surface layer where it is subject to exchange with the atmosphere, and this effect will vary between different environments depending on the amount and form of the biomass. While SAV is known to play a significant role in carbon cycling in the water and sediment (Abdolahpour et al., 2018; Adams et al., 2016), the effect of SAV on stratification is rarely considered in aquatic ecosystem models (Nakayama, Nakagawa, et al., 2020), particularly those used for carbon cycle investigations. Furthermore, the target areas of "blue carbon" research have mainly focused on marine and coastal ecosystems, with less attention paid to inland waters, such as freshwater or coastal lakes that can experience high vegetation densities and persistent stratification. There is therefore a need for improved methods for simulating blue carbon and carbon capture and storage processes that are applicable to freshwater lakes and coastal ecosystems.

In order to accurately represent carbon flows in these models, the mechanisms by which SAV suppresses vertical mixing and mediates the carbon dioxide flux from the vegetation canopy need to be considered. SAV is known to affect water circulation, and an array of numerical simulation models to enable analysis of a three-dimensional flow field has been developed (Weitzman et al., 2015; Zeller et al., 2014). For example, since the motion of submerged aquatic plants within a canopy controls mass transport, a SAV model that can capture the deflection of vegetation elements is required to resolve how much carbon is being absorbed (Nepf, 2012). Nakayama, Komai, et al. (2020) successfully developed a SAV model that included the feedback between vegetation movement and the flow field by integrating it with a three-dimensional hydrodynamic model and considering the drag, friction, buoyancy, and elastic forces associated with the vegetation elements. However, because their SAV model precisely simulated each element, including differences among the branches and leaf segments, its runtime cost was noted as being prohibitive for field-scale applications to lakes or coastal areas. To improve the implementation time for use in biogeochemical studies, methods are necessary to adapt this high-resolution model approach by integrating different "bundles" of submerged aquatic plants into a more practical subgrid-scale SAV parameterization.

On the other hand, spatially integrated vertical one-dimensional models have been used to investigate mass transport and water quality in lakes or enclosed coastal basins (Casamitjana et al., 2019; Hipsey et al., 2019; H. F. Jones et al., 2018) for some time. They have the advantage of resolving vertical mass transport while spatially integrating more complex three-dimensional phenomena created by horizontal gradients, such as density intrusions due to inflows (Imberger et al., 1978; Yeates et al., 2013). Due to the fast computational speed of models such as DYRESM and GLM, they are well suited for the simulation of water quality and carbon cycling in enclosed water bodies, and for longer-term climate change projections (Ladwig et al., 2021; Trolle et al., 2012; Zhang et al., 2020). Since spatially integrated models have had difficulty analyzing vertical convection induced by the horizontal water temperature differences, Okely and Imberger (2007) and Zhou et al. (2021) have contributed various methodological improvements, including the recent development of multibasin simulation capability (MB-DYRESM) able to parameterize more natural three-dimensional phenomena. For the purposes of investigating the dynamics of carbon capture and storage in enclosed aquatic ecosystems with dense vegetation and strong stratification over long time periods, spatially integrated models can serve as a useful approach of intermediate complexity. However, to date they have not specifically resolved the feedback between the vegetation canopy, water mixing, and carbon exchange.

In both vegetated and nonvegetated aquatic ecosystems, sediment respiration can be a dominant driver of vertical gradients in DIC, and this can be highly site specific (Bauer et al., 2013). For example, Lehrter et al. (2012) demonstrated that understanding the DIC flux from the sediment was crucial for clarifying respiration and the cause of bottom hypoxia in the mouth of the Mississippi River. Also, Karle et al. (2007) suggested the importance of understanding the DIC from the bottom sediment, which is not negligible when understanding the controls on metabolism in coastal areas. In shallower well-lit waters, particulate organic matter tends to accumulate to higher levels within the sediment, due to both local vegetation litter inputs and also because SAVs inhibit the mass transport between the upper and lower layers due to the formation of stratification, with the net effect of substantially higher carbon dioxide fluxes from vegetated bottom sediments (Adams et al., 2016; Baird et al., 2016; Trolle et al., 2014).

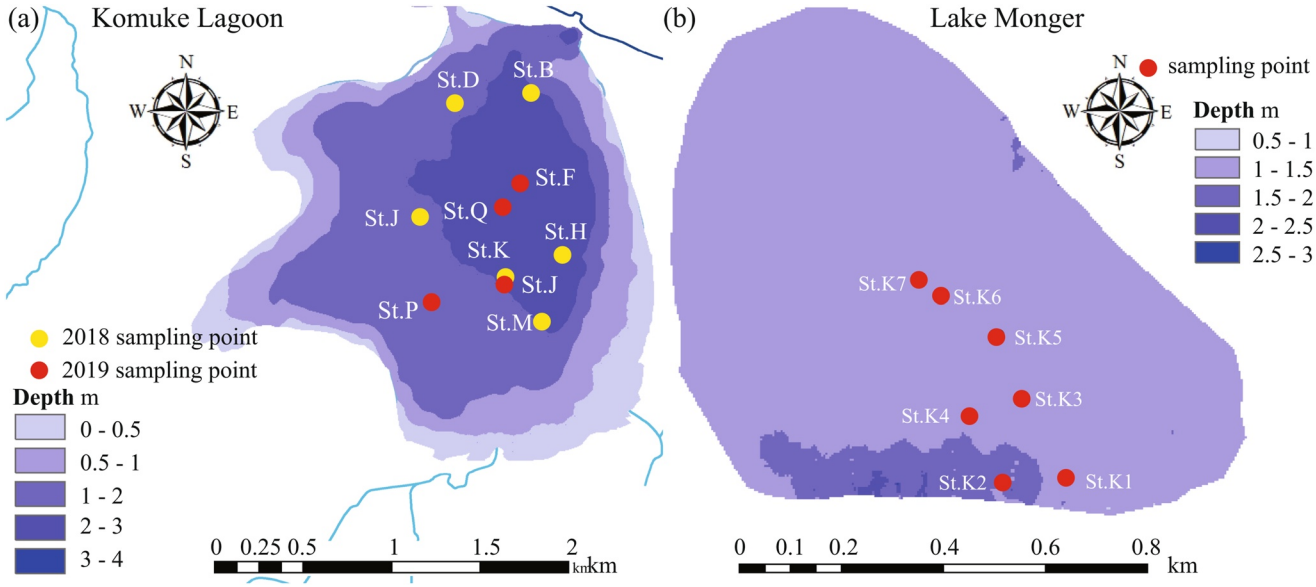

Figure 1. Sampling stations in (a) Komuke Lagoon and (b) Lake Monger.

Thus, in order to accurately estimate carbon release and capture associated with SAV, it is essential to clarify not only the respiration and photosynthesis effects on DIC due to SAV productivity, and also the DIC flux associated with respiration of the bottom sediments, but also the nature of mass transport associated with the SAV canopy, mediated by the effect of vegetation on stratification and vertical motions across the vegetation boundary layer. This study aims at developing a spatially integrated model to estimate inorganic carbon dynamics suitable for stratified waters and able to accommodate different vegetation canopy properties. To elucidate the interplay of the various processes and their relevance within both coastal and freshwater ecosystems, we applied the model at two different case studies: Komuke Lagoon (Hokkaido, Japan) and Lake Monger (Western Australia, Australia). Komuke Lagoon is a typical eutrophic coastal (saline) lagoon with *Zostera marina*, and Lake Monger is a typical eutrophic freshwater lake with *Potamogeton crispus*. Both sites are enclosed water bodies that experience seasonal coverage with SAVs from spring to autumn, however, they experience different stratification phenology and plant densities. Using the model, we compare Komuke Lagoon and Lake Monger in terms of the controls on DIC transport and uptake and net SAV production. First, the effect of stratification due to SAV was investigated by means of field observations in both sites. Second, the DIC productivity equation in Nakayama, Komai, et al. (2020), which was developed for *Z. marina* in Komuke, was extended to also fit *P. crispus* in Lake Monger. Third, a conceptual two-layer steady-state DIC model was applied to estimate the DIC flux from the bottom sediment. Lastly, the derived source and sink terms of DIC were applied within a spatially integrated numerical model of hydrodynamics, vegetation and DIC (termed "SiDIC"). The vegetation model extends the flexible leaf model of Nakayama, Nakagawa, et al. (2020) by integrating shoot density in each computational cell as a "bundle" of submerged aquatic plants able to moderate water column mixing. The coupled model resolves the effect of SAV metabolism and drag effects on DIC vertical profiles under dynamic hydrological conditions, and is validated against measurements from the sites before being applied to demonstrate the sensitivity of water column DIC to different environmental conditions.

2. Method

2.1. Site Selection and Field Investigations

Komuke Lagoon is located in eastern Hokkaido along the Okhotsk Sea (North latitude 44°15′30″, East longitude 143°30′20″; Figure 1a). The water area is 4.84 km^2, the mean water depth is 1.2 m, and the maximum depth is 3.8 m. Komuke Lagoon consists of three enclosed basins and is a typical lagoon, which can trap nutrients. Eelgrass (*Z. marina*) inhabits the subtidal zones and contributes to sequestering organic carbon in the sediments (K. Watanabe & Kuwae, 2021). The field observations we conducted in 2018 showed that the salinity range was about 20–34 because of the greater seawater exchange with the Okhotsk Sea than river inflow. Also, the mean

values of nitrate nitrogen, ammonium nitrogen, and phosphate phosphorus were observed to be approximately 0.0033, 0.0048, and 0.032 mg L^{-1}, respectively, from spring to autumn. The tidal range of Komuke Lagoon is only 0.5 m because of the narrow 15 m width of the tidal inlet. Chlorophyll *a* (Chl. *a*) is approximately 3 μg L^{-1}. For this reason, calm water conditions are usual in Komuke Lagoon, and the eelgrass population is widely distributed without the significant influence of phytoplankton. Also, the effect of the attached organisms on leaves is negligibly small on the partial pressure of carbon dioxide. In Komuke Lagoon, epiphytes are more likely to attach to leaves during snowmelt flood periods from March to April when the SAV leaf length is short and nutrients are higher. However, since the large river inputs are not occurring from spring to summer and the currents induced by tides are relatively strong, this prevents epiphyte build-up as the SAV canopy develops. Therefore, Komuke Lagoon is ideal for investigating the stratification effect on carbon absorption due to the SAV meadow. The meadows and tidal flats create high-quality habitats for the migrations of birds. The field observations were conducted on the 8 August 2018 and the 22 July 2019. Vertical profiles of water temperature, dissolved oxygen (DO), and Chl. *a* were measured with a vertical interval of 1 cm using an AAQ-RINKO profiler (JFE Advantech). The water adjacent to the water surface (10 cm below the surface) and the bottom (5 cm above the sediment) was sampled using a Van Dorn water sampler (Miyamoto Riken Ind. Co.). Mercuric chloride (250 μL) was added to the sampled water (250 mL) to fix DIC and total alkalinity (TA). DIC and TA were measured using an ATT-15 titration analyzer with about 5 μmol L^{-1} of precisions (Kimoto Electric Co.).

Lake Monger is located in Perth in Western Australia (South latitude 31°55′45″, East longitude 115°49′35″; Figure 1b). The water surface area is 0.68 km^2, the mean water depth is from 0.3 m in autumn to 1.2 m in spring, and the maximum depth is 2.0 m. *Potamogeton crispus* is the dominant aquatic vegetation in Lake Monger, which grows in lakes and rivers in a wide range of climates. *Potamogeton crispus* typically initiates growth in the middle of the lake densely by the beginning of spring and spreads toward the lake edges by early summer. In late summer, the bottom anoxia due to the dense submerged vegetation is revealed to form a ring-shaped pattern in *P. crispus* beds (Vilas, Marti, et al., 2017). Lake Monger receives inflows from various stormwater drains, and discharge to the groundwater is the main outflow. Therefore, the water depth does not change as substantially as in Komuke Lagoon. The annual mean values of nitrate nitrogen, ammonium nitrogen, and phosphate phosphorus are about 0.077, 0.296, and 0.118 mg L^{-1}, respectively, which provide enough nutrients for *P. crispus* to grow into very dense stands. The maximum value of Chl. *a* is more than 100 μg L^{-1} without *P. crispus*, but it is less than 10 μg L^{-1} when the *P. crispus* canopy has fully developed, resulting in limited epiphytes on the leaves as a consequence. A field campaign was conducted on the 27 November 2019, which was a sunny and calm day. Vertical profiles of water temperature, DO, and Chl. *a* were measured using an AAQ-RINKO profiler, in the same manner as for the Komuke Lagoon. The water adjacent to the water surface (10 cm below the surface) and the bottom (10 cm or 20 cm above the sediment) was sampled using a hand pump without air. Mercuric chloride (100 μL) was added to the sampled water (100 mL), and samples were analyzed for DIC and TA using the same ATT-15 analyzer as used for the Komuke Lagoon measurements. TA and DIC values were calibrated against certified reference material (Batch AO; TA = 2,257.6 ± 0.9 μmol kg^{-1}, and DIC = 1,987.1 ± 0.68 μmol kg^{-1} from KANSO Technos, Japan).

2.2. Laboratory Experiments and Calculations

The bulk method was used to estimate carbon dioxide flux from the water surface to the atmosphere as follows:

$$F_a = kS(pCO_2 - pCO_{2\,air}) \quad (1)$$

where F_a is the carbon dioxide flux from the water surface to the atmosphere (μmol m^{-2} s^{-1}), S is the solubility of carbon dioxide (mol m^{-3} atm^{-1}), pCO_2 is the partial pressure of carbon dioxide in water (μatm), $pCO_{2\,air}$ is the partial pressure of carbon dioxide in the atmosphere (μatm; Weiss, 1974), and k is a gas exchange parameterization (m s^{-1}) defined as (Wannikhof, 1992)

$$k = 0.39U_{10}^2\left(\frac{Sc}{660}\right)^{-0.5} \quad (2)$$

where U_{10} is the wind speed at 10 m from the water surface (m s^{-1}); Sc is the Schmidt number defined as (Jähne et al., 1987)

$$Sc = A - Bt + Ct^2 - Dt^3 \quad (3)$$

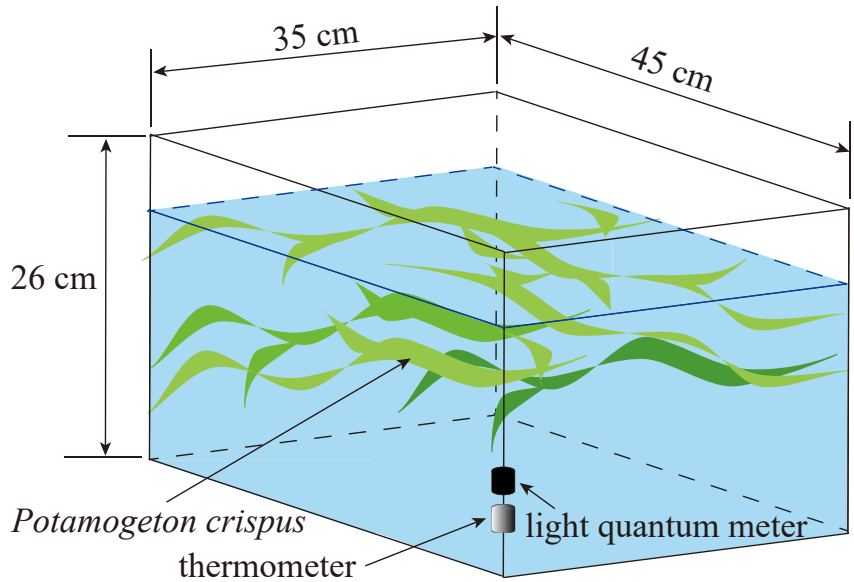

Figure 2. Schematic diagram of the laboratory experiment tank containing *Potamogeton crisps*. The laboratory experiment was conducted in Perth, Australia, on 28–30 November in 2019. Density of submerged aquatic vegetation (SAV) was 2,000 shoots m^{-2}. Mean leaf length was 0.76 m.

where A, B, C, and D are the values empirically determined by gas type and the ratio of seawater to freshwater. In seawater and when the gas is carbon dioxide, $A = 2073.1$, $B = 125.62$, $C = 3.6276$, and $D = 0.043219$. In freshwater, $A = 1911.1$, $B = 118.11$, $C = 3.4527$, and $D = 0.04132$. t is water temperature (°C).

A DIC metabolism equation for *Z. marina* in Komuke Lagoon has been previously parameterized considering respiration, photosynthesis, and water temperature effects (Nakayama, Komai, et al., 2020), however, no such equation has been developed for *P. crispus* in Lake Monger. A controlled laboratory experiment was therefore conducted, which was then used to define the necessary coefficients for *P. crispus* metabolism (Section 2.3). We prepared a water tank filled with sampled water from Lake Monger, and 100 shoots of *P. crispus* were placed in the tank (Figure 2). The roots of *P. crispus* were covered with vinyl sheets to avoid oxygen consumption by oxygen-demanding substances contained in the sediment and DIC release from the bottom sediment. Two thermometers (SERA Diver; Eijkelkamp Co., Ltd.) and two light quantum loggers (DEFI2-L; JFE Advantech Co., Ltd.) were employed in the water tank, recording every 10 min. The experiment was started at 6:00 p.m. on the 28 November 2019, when photosynthesis was inactive, and continued for 48 hr. The partial pressure of carbon dioxide (pCO_2) was measured every 5 min using a Mini CO_2 sensor (Pro Oceanous Co.). Water was sampled 3 times a day using 100 mL vial bottles with 100 µL mercuric chloride. DIC and TA were measured using an ATT-15 titration analyzer (Kimoto Electric Co.). The measured TA was used to determine whether TA can be assumed to be constant or not. DIC was estimated from pCO_2 and TA obtained from water samples by using the chemical equilibrium equation (Zeebe & Wolf-Gladrow, 2001), which was verified by comparing DIC from water samples with an r^2 of 0.99. Also, we used Millero (2010) in CO2sys, suggesting no significant difference between Millero (2010) and Zeebe and Wolf-Gladrow (2001). Note that the calculated DIC from pCO_2 and TA using chemical equilibrium equation could introduce error as much as 20%.

2.3. Evaluation of Coefficients of SAV Metabolism

The equation for DIC metabolism was successfully developed by Nakayama, Komai, et al. (2020) for *Z. marina* in Komuke Lagoon, building on the work of previous studies (Beca-Carretero et al., 2018; Burkholz et al., 2019; Drew, 1979; Goodman et al., 1995; Holmer & Bondgaard, 2001; Marsh et al., 1986; Olesen & Sand-Jensen, 1993; Staehr & Borum, 2011; Touchette, 1999; Zimmerman et al., 1995, 1997). Using this approach, DIC is resolved as the balance of respiration and light-mediated productivity:

$$\frac{d}{dt}(\mathrm{DIC}) = R_{\mathrm{A}}\exp\left(-\frac{E_{\mathrm{aR}}}{T_{\mathrm{w}}R}\right) - P_{\psi}\tanh\left(\frac{\alpha_{\psi}I}{P_{\psi}}\right)R_{\mathrm{P}}\exp\left(-\frac{E_{\mathrm{aP}}}{T_{\mathrm{w}}R}\right) \quad (4)$$

Table 1
Parameters of the DIC Equation for Z. marina in Komuke Lagoon and P. crispus in Lake Monger

Parameters	Komuke Lagoon (Nakayama, Komai, et al., 2020)	Lake Monger
Leaves (shoot^{-1})	4	1
SAV density in laboratory experiments (shoot m^{-2})	100	2,000
Leaf carbon weight (g-C m^{-2}) leaf length = 1.0 m	103	214
Carbon weight (g-C shoot^{-1}) leaf length = 1.0 m	1.03	0.107
Leaf nitrogen weight (g-N m^{-2}) leaf length = 1.0 m	4.4	9.5
R_A (μmol kg^{-1} hr^{-1})	1.04×10^{17}	3×10^{23}
E_{aR} (m^2 kg s^{-2})	1.52×10^{-19}	2.04×10^{-19}
P_ψ (μmol kg^{-1} hr^{-1})	21.5	87.7
R_P	2.30×10^{7}	2.28×10^{18}
α_ψ (m^2 s kg^{-1} hr^{-1})	21.5/200	87.7/90
E_{aP} (m^2 kg s^{-2})	0.69×10^{-19}	1.71×10^{-19}

where DIC (μmol kg^{-1}) is the dissolved inorganic carbon for 100 shoots m^{-2}, R_A (μmol kg^{-1} hr^{-1}) is the parameter for respiration, E_{aR} (m^2 kg s^{-2}) is the activation energy for respiration, T_w (K) is the water temperature, R (m^2 kg s^{-2} K^{-1}) is the Boltzmann constant (1.380649×10^{-23}), P_ψ (μmol kg^{-1} hr^{-1}) and α_ψ (m^2 s kg^{-1} hr^{-1}) are the parameters for photosynthesis, I (μmol m^{-2} s^{-1}) is the photon flux density, R_p is the parameter for photosynthesis, and E_{aP} (m^2 kg s^{-2}) is the activation energy for photosynthesis.

The parameters of the above DIC equation for 100 shoots m^{-2} in Komuke Lagoon were previously determined and are summarized in Table 1. For Lake Monger, the parameters for the respiration term in Equation 4, R_A and E_{aR}, were obtained first by using data from the laboratory experiments (Figure 6) by assuming photosynthesis activity is negligible from sunset to sunrise when photon flux density is zero. Second, the parameters for photosynthesis were obtained by considering the daytime photon flux density and DIC change, in order to resolve parameters R_A and E_{aR}; these are also summarized in Table 1. Dry weight was measured after heating by an electric oven at 105°C for 24 hr. Dried sample was ground using a mortar and pestle and elemental carbon content analyzed using a CHNS analyzer.

2.4. A Simple Steady-State Two-Layer DIC Model to Estimate the Sediment DIC Flux

There is a possibility that SAV enhances stratification and thus inhibits the DIC flux between the upper and lower water layers (Adams et al., 2016; Nakayama, Nakagawa, et al., 2020; Vilas, Adams, et al., 2017). As a result, a two-layer fluid is formed, causing a significant difference in DIC between the upper and lower layers. Nakayama et al. (2010) demonstrated a simple two-layer model to analyze DO in an enclosed basin which we use as the basis to develop a conceptual DIC model for a two-layer fluid. This enabled us to investigate the vertical DIC fluxes and specifically allowed us to separate the bottom sediment flux from the biochemical change in DIC due to SAV (Figure 3).

The layer thicknesses were determined by using the vertical density profile from the field observations in Komuke Lagoon and Lake Monger. In the upper layer, the carbon dioxide flux between the water surface and atmosphere (Equation 1), the respiration and photosynthesis due to SAV (Equation 4), and the DIC flux between the upper and lower layers were considered. The DIC flux between the upper and lower layers, the respiration and photosynthesis due to SAV, and the DIC flux from the bottom sediment are included in the lower layer. The horizontal DIC fluxes were also included using a horizontal exchange coefficient, α_{EX}. Komuke Lagoon was covered by SAVs during field observations and therefore we set $\alpha_{EX} = 1.0$. However, SAVs existed patchwise in Lake Monger, suggesting that α_{EX} should be less than 1.0. Thus, the conceptual two-layer DIC model is proposed:

$$\rho_w V_U \frac{\partial(\mathrm{DIC}_U)}{\partial t} = -\alpha_{EX} V_U \mathrm{NEP}_U + \rho_w A_h w_e \mathrm{DIC}_L - F_a A_h \quad (5)$$

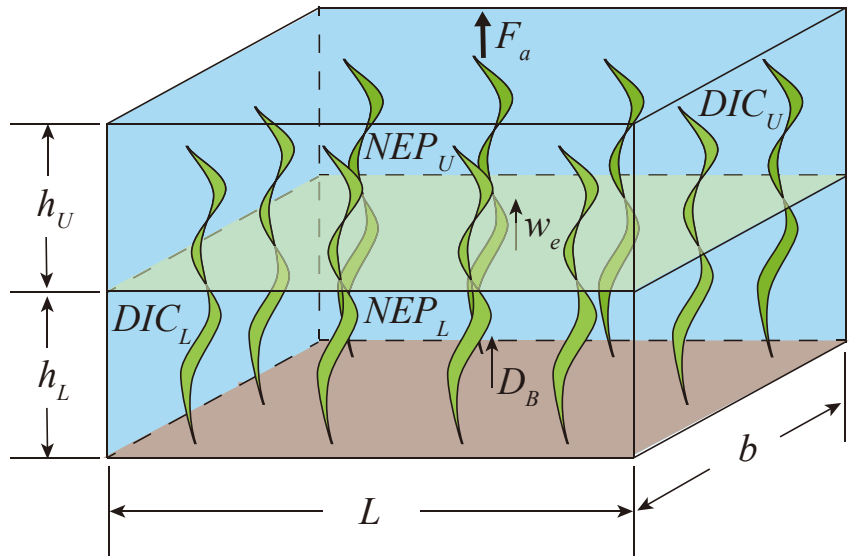

Figure 3. Schematic diagram of a conceptual dissolved inorganic carbon (DIC) model. Here, h_U is the thickness of the upper layer (m) and h_L is the thickness of the lower layer (m), DIC_U is the DIC density at the upper layer (μmol kg^{-1}), DIC_L is the DIC density at the lower layer (μmol kg^{-1}), w_e is the entrainment velocity at the boundary (m s^{-1}), NEP_U is the net ecological production (NEP) at the upper layer (μmol L^{-1} s^{-1}), NEP_L is the NEP at the lower layer (μmol L^{-1} s^{-1}), F_a is the carbon dioxide flux between the water surface and atmosphere (μmol m^{-2} s^{-1}), and D_B is the DIC flux from the bottom of a lake (μmol s^{-1}). h_U, h_L, DIC_U, DIC_L, and F_a are obtained from the field observations. NEP_U and NEP_L are given using the DIC equation. L and b are given 1 m, respectively.

$$\rho_w V_L \frac{\partial(\mathrm{DIC_L})}{\partial t} = -\alpha_{EX} V_L \mathrm{NEP_L} - \rho_w A_h w_e \mathrm{DIC_L} + D_B A_h \tag{6}$$

Here, ρ_w is the water density (=1 kg L^{-1}), α_{EX} is the horizontal exchange coefficient (−), V_U is the volume at the upper layer (m^3), NEP_U is the net ecological production (NEP) at the upper layer (μmol m^{-3} s^{-1}), A_h is the area of the boundary surface (m^2), w_e is the entrainment velocity at the boundary (m s^{-1}), DIC_L is the DIC concentration at the lower layer (μmol $kg^{-1} = 12 \times 10^{-3}$ mg L^{-1}), DIC_U is the DIC concertation within the upper layer (μmol k $g^{-1} = 12 \times 10^{-3}$ mg L^{-1}), F_a is the carbon dioxide flux between the water surface and atmosphere (μmol m^{-2} s^{-1}), V_L is the volume at the lower layer (m^3), NEP_L is the NEP at the lower layer (μmol m^{-3} s^{-1}), and D_B is the DIC flux from the bottom sediment (μmol m^{-2} s^{-1}). NEP_U and NEP_L are obtained using the equations described next, and DIC_U, DIC_L, and F_a were set from the field observations as outlined above. The significant point of the model is that the decomposition of sediment organic matter is included as the DIC flux from the bottom sediment into the lower layer, D_B, and remains unknown. Note that water temperature and salinity are not modeled in a manner similar to DIC because water temperature and salinity do not change due to the biochemical reactions and the horizontal fluxes are substantial.

Assuming that the DIC profile has reached a pseudo-steady-state condition, $\partial(\mathrm{DIC})/\partial t = 0$, Equations 7 and 8 simplify to

$$0 = -\alpha_{EX} h_U \mathrm{NEP_U} + w_e \mathrm{DIC_L} - F_a \tag{7}$$

$$0 = -\alpha_{EX} h_L \mathrm{NEP_L} - w_e \mathrm{DIC_L} + D_B \tag{8}$$

where h_U is the thickness of the upper layer (m) and h_L is the thickness of the lower layer (m). The significance of the pseudo-steady-state assumption is discussed later in Section 4.

NEP_U and NEP_L are the temporal change in DIC due to respiration and photosynthesis due to the submerged aquatic plants, respectively, using the DIC metabolism equation. They are computed following Nakayama, Komai, et al. (2020):

$$\mathrm{NEP_U} = -\mathrm{NEPR_U} + \mathrm{NEPP_U} = -k_U \frac{h_{AU}}{h_U} R_A \exp\left(-\frac{E_{aR}}{T_w R}\right) + k_U \frac{h_{AU}}{h_U} P_\psi \tanh\left(-\frac{\alpha_\psi I_{Uave}}{P_\psi}\right) R_P \exp\left(-\frac{E_{aP}}{T_w R}\right) \tag{9}$$

$$\mathrm{NEP_L} = -\mathrm{NEPR_L} + \mathrm{NEPP_L} = -k_\mathrm{L}\frac{h_\mathrm{AL}}{h_\mathrm{L}}R_\mathrm{A}\exp\left(-\frac{E_\mathrm{aR}}{T_\mathrm{w}R}\right) + k_\mathrm{L}\frac{h_\mathrm{AL}}{h_\mathrm{L}}P_\psi\tanh\left(-\frac{\alpha_\psi I_\mathrm{Lave}}{P_\psi}\right)R_\mathrm{P}\exp\left(-\frac{E_\mathrm{aP}}{T_\mathrm{w}R}\right) \quad (10)$$

where I_Uave and I_Lave are average photon flux density in the upper or lower layers (μmol $\mathrm{m^{-2}\ s^{-1}}$), k_U and k_L are the proportion of SAV density compared to the laboratory experiment in the upper or lower layers, h_AU and h_AL are the length of submerged aquatic plants in the upper or lower layers (m), $\mathrm{NEPR_U}$ and $\mathrm{NEPR_L}$ are the change in DIC due to respiration by SAV in the upper or lower layers (μmol $\mathrm{kg^{-1}\ s^{-1}}$), and $\mathrm{NEPP_U}$ and $\mathrm{NEPP_L}$ are the change in DIC due to photosynthesis by submerged aquatic plants in the upper or lower layers (μmol $\mathrm{kg^{-1}\ s^{-1}}$).

The mean photon flux density in the upper and lower layers is given by (Nakayama, Komai, et al., 2020)

$$I_\mathrm{Uave} = I_0\frac{1}{h_\mathrm{U}}\int_0^{h_\mathrm{aU}}\exp[-k_\mathrm{E}(h_\mathrm{U}-z)]dz \quad (11)$$

$$I_\mathrm{Lave} = I_0\frac{1}{h_\mathrm{L}}\int_0^{h_\mathrm{aL}}\exp[-k_\mathrm{E}(h_\mathrm{U}+h_\mathrm{L}-z)]dz \quad (12)$$

where I_0 is the solar irradiance (μmol $\mathrm{m^{-2}\ s^{-1}}$), k_E (=0.5) is the extinction coefficient ($\mathrm{m^{-1}}$), h_U is the thickness of the upper layer (m), and h_aU and h_aL are the existence length of submerged aquatic plants from the bottom of the upper layer and lower layer, respectively.

The unknown values are the entrainment velocity (w_e) and DIC flux from the bottom sediment in Equations 7 and 8. To solve for these, we first obtain the entrainment velocity from Equation 7, and then calculate the DIC flux from the bottom sediment from Equation 8.

2.5. A Dynamic SiDIC Model Considering SAV

In the previous Section 2.4, the conceptual basis for the two-layer model was developed, and, under the assumption of steady-state conditions, the DIC flux from the bottom sediment was resolved by using the sampling results from the upper and lower layers. From the viewpoint of climate change, it is necessary to develop a model that can simulate long-term projection to investigate carbon dioxide flux considering anthropogenic carbon emissions, which would enable us to obtain and interpret more detailed information, such as the vertical profile of DIC. Therefore, we extend the above analysis to develop a spatially (horizontally) integrated DIC (SiDIC) numerical model suitable for shallow water areas, which is able to clarify the vertical and temporal changes of DIC. The base model is a three-dimensional environmental model, Fantom (Nakayama, Sato, et al., 2020; Nakayama et al., 2014, 2016). The governing equation is the Navier-Stokes equation, and object-oriented programming is used. A generic length-scale equation model was also employed to evaluate how the vertical mixing affected the water's mass and energy transport (W. P. Jones & Launder, 1972; Umlauf & Burchard, 2003). We applied the fully coupled hydrodynamic-SAV model, based on the discrete element method (DEM), considering the drag, lift, friction and elastic forces, and buoyancy, to resolve vegetation motion (Nakayama, Nakagawa, et al., 2020). Using the DEM approach, each leaf can be divided into connected separate segments, which together are used to compute the Lagrangian blade dynamics (Figure 4b). All forces associated with the interaction with the flow are assumed to apply at the node that connects each segment to obtain node velocities with a limiting condition of a segment length. The SAV model maps the flow velocity from the hydrodynamic model cell at the appropriate location, and returning the friction and drag terms to the Fantom accordingly.

In Komuke Lagoon, the density of *Z. marina* is 25 shoots $\mathrm{m^{-2}}$, meaning that ~500 shoots should be considered in one vertical column. Nakayama, Nakagawa, et al. (2020) revealed that the time step for the simulation of SAV with individual shoot motion resolved should be about 0.050 s, which for a field-scale simulation would create an excessive runtime cost (Figure 4c). Therefore, in this study, we introduce a grid-integrated SAV (GiSAV) model, whereby 500 submerged aquatic plants (shoots) are integrated into one bulk unit in each grid (Figure 4d). Namely, numerous SAVs in each column move due to waves and current and react to the flow in the same way by assuming that the external force is given equally in each column. In this approach, the force from the flow to a GiSAV unit is given the same as in the original hydrodynamic-SAV model; however, the feedback from the GiSAV to the flow is upscaled based on the actual shoot number, meaning that the force from the GiSAV to the flow was given by multiplying the drag from a single shoot by the actual shoot number per cell. For example, if

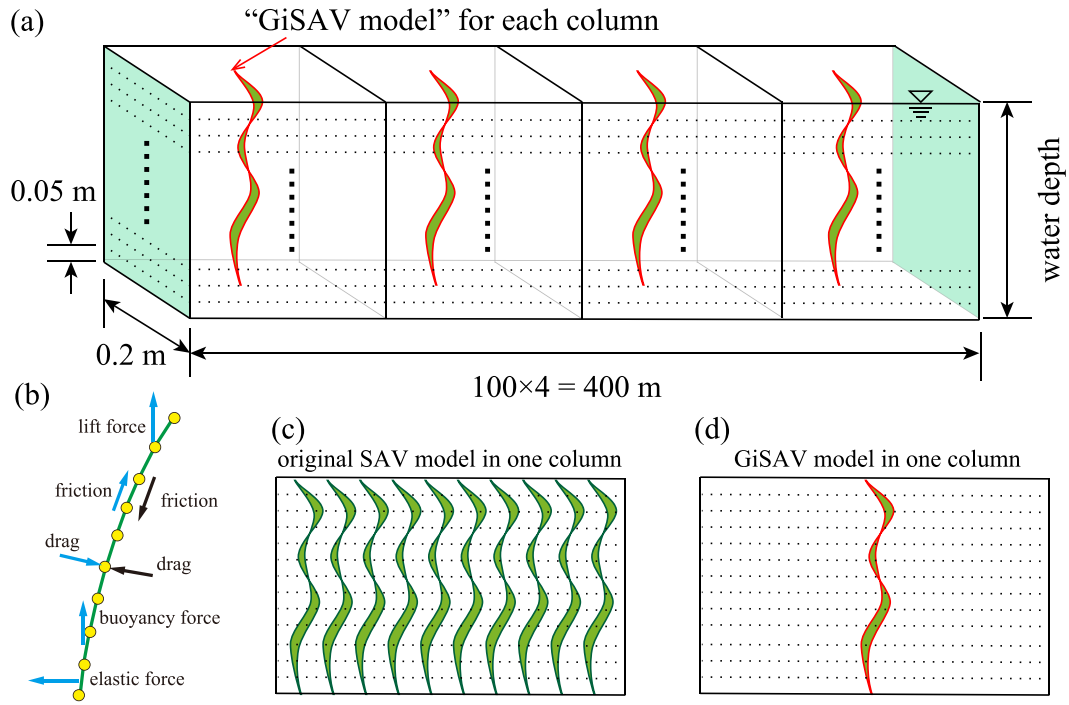

Figure 4. Spatially integrated dissolved inorganic carbon (SiDIC) model. Dotted lines indicate the boundary of cells in each column. (a) Computational domain for SiDIC model. (b) Schematic diagram of submerged aquatic vegetation (SAV) model. Blue and black arrows indicate forces from flow to SAV and from SAV to flow. (c) Original SAV model: all SAVs must be modeled in each column. (d) Grid-integrated SAV (GiSAV) mode: a bundle of submerged aquatic plants is integrated into one SAV bulk unit in each column.

100 SAVs are integrated into one GiSAV unit within a vertical column, the drag force from one GiSAV to the horizontal and vertical velocity components is given by multiplying the actual shoot number (=100). To ensure the total drag imparted on the fluid using the GiSAV model was equivalent to the SAV model, numerical simulations were conducted, giving 500 SAVs in each column. The validity of the GiSAV model approach was verified by comparing it with the 500 SAV model results.

In addition to the effect of SAV on the flow velocities, the model resolves the DIC concentration and, aside from advection and mixing, resolves the change in DIC in each cell due to the SAV based on Equation 4 and DIC flux from the bottom sediment and atmospheric exchange. Photon density flux and water temperature are necessary to compute the change in DIC using Equation 4, in which water temperature was given from the Fantom at the appropriate cell location of SAV's node. Photon density flux was computed using the extinction coefficient based on the field observations, meaning that the photon density flux was the maximum at the water surface and decreased with the water depth exponentially. The simple steady-state two-layer DIC model results gave DIC flux from the bottom sediment. DIC flux for the atmospheric exchange was given from the field observation results using Equation 1.

To investigate the effect of leaf length on DIC, the SiDIC model was applied to Komuke Lagoon using field observations at St. J, St. P, and St. Q on the 22 July in 2019, because the ratio of leaf length to total water depth ranged from 0.24 to 1.0 at those locations. The field observations in August 2018 were not used, because the wind speed was too high to investigate the effect of the SAV on the process of stratification. Since Fantom reproduces a three-dimensional domain combining vertical columns horizontally, we prepared four straight columns using a sizable horizontal grid size (Figure 4a). The grid sizes were 100 m in the longitudinal direction and 0.2 m in spanwise width. The vertical cell height was given 0.05 m. Because a sizable horizontal grid size was applied, the hydrostatic assumption was used, and a time step of 10.0 s was applied. The limitation of the hydrostatic assumption was investigated, resulting in the high applicability of the hydrostatic model when wind stress is given at the water surface without causing significant wind waves (Matsumoto et al., 2020). Note that unsteady unidirectional current may also induce nonhydrostatic pressure, which could play a role in the bend of leaf blades

and the change in velocity inside SAV meadows, however, we assumed this effect to be relatively insignificant for the comparisons being undertaken in this study. DIC was assumed not to change in the spanwise direction. In this study, SAV consisted of 5 cm segments. Numerical simulations were carried out from 3:00 on the 22 July 2019 to analyze the field observations at 13:00 on the 22. The initial condition was given by assuming that the water was vertically well mixed during nighttime. The water temperature and DIC values were determined by considering that the values are similar to those without SAVs. Note that the initial DIC may be slightly too small because of the respiration during nighttime. Meteorological data were obtained by field observation (Automatic Meteorological Data Acquisition System of Japan Meteorological Agency) at Monbetsu and Abashiri stations (available from https://www.jma.go.jp/jma/en/Activities/observations.html), and the density of SAV was given as 25 shoots m^{-2} based on our field observations.

Furthermore, we attempted to investigate the hourly change in DIC by giving several different conditions regarding leaf length and wind speed, assuming the conditions of *Z. marina*. Three leaf lengths were used, 0.5, 1.0, and 1.5 m, with a total water depth of 1.5 m. Also, three different wind speeds were used, 2, 4, and 6 m s^{-1}. In addition, since the process of stratification is associated with wind speed and the density of submerged aquatic plants, we considered three densities of SAV shoots: 100 shoots, m^{-2} (10 cm spatial interval), 25 shoots, m^{-2} (20 cm spatial interval), and 11 shoots, m^{-2} (30 cm spatial interval). A total of 27 simulations were therefore examined, and each was run for 4 days by giving diurnal external forcing, with the last day as used for the investigation. To interpret the influence of hourly DIC changes on pCO_2, we computed pCO_2 by assuming that the maximum pCO_2 was 300, 400, and 500 µatm when the maximum DIC occurred. Three different maximum pCO_2 was given by changing the value of TA and can enable us to understand the uncertainty of pCO_2 fluctuations due to the initial setups. Note that DIC flux from the bottom sediment was set as 518.4 mg-C m^{-2} day^{-1}.

3. Results

3.1. Influence of SAV on Stratification and DIC

The ratios of the length of *Z. marina* to the total water depth were 0.7 m/1.1 m, 1.1 m/1.0 m, and 0.3 m/1.25 m at St. J, St. P, and St. Q of Komuke Lagoon in 2019, respectively, enabling us to estimate the effect of SAV height on stratification. Therefore, St. J, St. P, and St. Q were chosen to show the influence of SAV on stratification (Figure 5 and Table 2). Salinity was vertically and horizontally uniform and 33.4–34.1 excluding St. K in the entire Komuke Lagoon in both field observations in 2018 and 2019, suggesting that there is little effect of salinity change on DIC and TA because the seawater exchange between Komuke Lagoon and the Okhotsk Sea is larger than inflow discharge and dominates salinity in the entire lagoon. As the average wind speed during the field observation was 3.5 m s^{-1}, the shortest leaf length condition was well mixed and had vertically uniform water temperature, excluding a slight decrease in water temperature in the region from the bottom to a head of 0.2 m at St. Q. Although the leaf length was short at St. Q, DO was about 150% due to the photosynthesis of SAV. At St. J, where the leaf length is 0.7 m in a total water depth of 1.1 m, water temperature decreased significantly at a water depth of 0.5 m, suggesting that submerged aquatic plants enhanced the process of stable stratification. The stable stratification suppresses the vertical flux of DO between the upper and lower layers, resulting in a substantial increase in DO in the lower layer, excluding DO values adjacent to the bottom due to the consumption of DO by ecosystem respiration near the bottom sediment. At St. P, where *the Z. marina* reached the water surface, submerged aquatic plants reduced the energy contributed by wind, and the mixing depth was 0.4 m. Because SAV reached the water surface at St. P, DO had a higher percentage compared to the other stations. Unlike in 2019, there was no apparent stratification in 2018, because the average wind speed was more than 5.0 m s^{-1}.

Regarding pCO_2 estimated from DIC and TA in the upper layer in Komuke Lagoon, the value was 40.1 µatm at the water surface of St. P in 2019, where the *Z. marina* reached the water surface (Table 2). Hu and Cai (2013) and Simpson et al. (2022) revealed that DO, pH, and pCO_2 change in tandem in response to biological metabolism. The saturation of DO was more than 250% (more than 16 mg L^{-1}) at St. P, a higher percentage than other stations. This significant autotrophic condition reduces DIC, which lowers the pCO_2 more than the other stations. The second lowest pCO_2 was 103 µatm at St. J with a saturation of DO of 195% (more than 13 mg L^{-1}), which is higher than 150% (more than 10 mg L^{-1}) at St. Q with the pCO_2 of 278 µatm. The value of the saturated DO was 8 mg L^{-1}. The smaller the leaf length ratio to the total water depth, the greater pCO_2 adjacent to the water surface. For example, the partial pressures of carbon dioxide were 354.5 and 278.2 µatm at St. F and St. Q, respectively, where the leaf length is less than half of the total water depth. Although the leaves reached the water surface at all

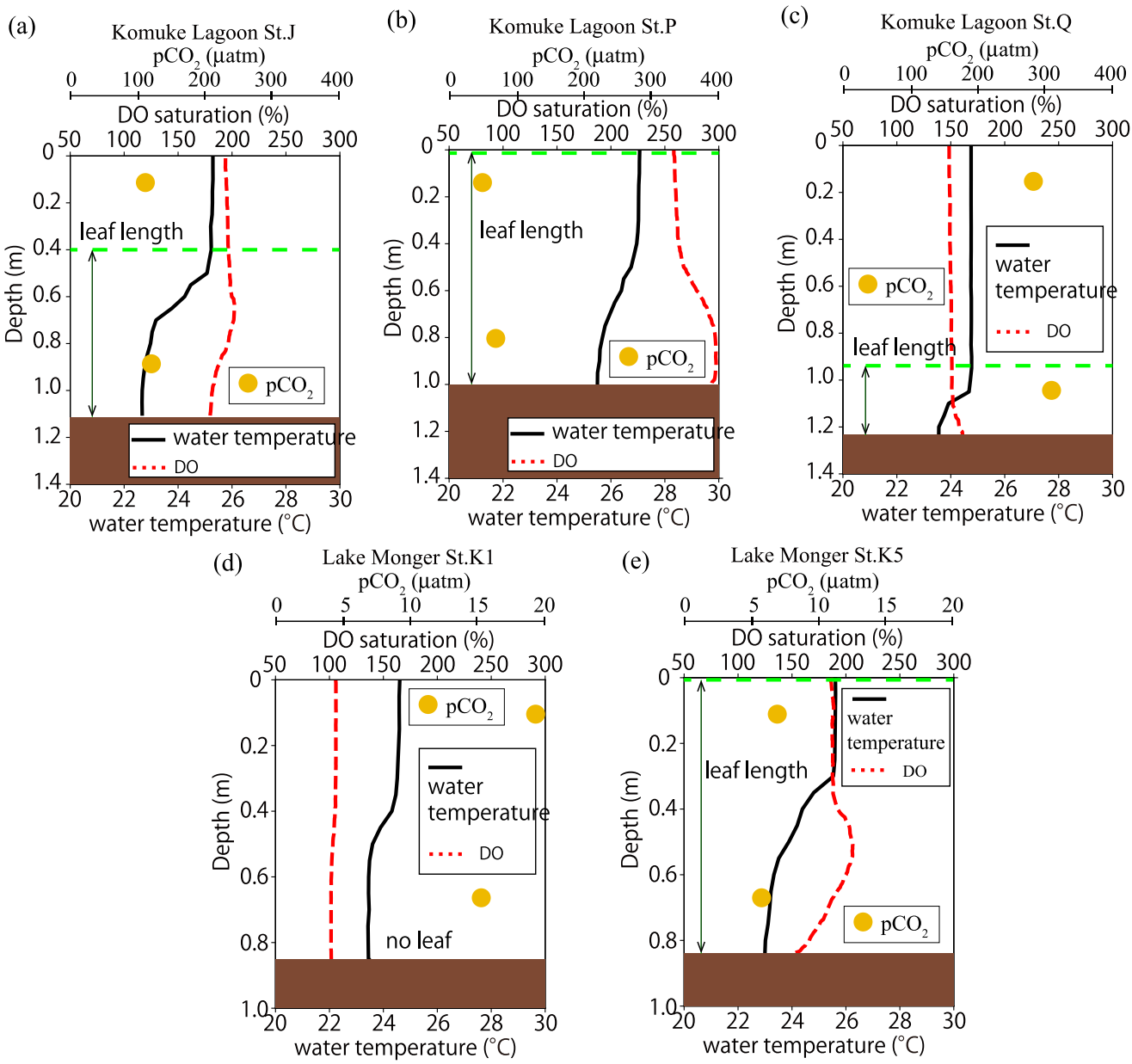

Figure 5. Vertical profile of water temperature, dissolved oxygen (DO), and pCO_2 measured at (a) St. J, (b) St. P, and (c) St. Q in Komuke Lagoon on the 22 July 2019, and at (d) St. K1 and (e) St. K5 in Lake Monger on the 27 November 2019. Green broken lines show the top height of the submerged aquatic vegetation (SAV) canopy.

stations of Komuke Lagoon in 2018, the spatial density of the *Z. marina* was smaller than in 2019, resulting in a slightly larger pCO_2 in 2018. For example, the smallest pCO_2 in the upper layer was 120.4 µatm in 2018 compared to 40.1 µatm in 2019. However, carbon dioxide flux at the water surface was more significant in 2018 than in 2019 because the average wind speed in 2018 was greater than that in 2019.

In comparison to Komuke Lagoon, pCO_2 was smaller in Lake Monger (Table 3). We confirmed that the pCO_2 values by Zeebe and Wolf-Gladrow (2001) almost agreed with those by Millero (2010) (Dickson, 1990; Dickson et al., 2007; Lewis & Wallace, 1998; van Heuven et al., 2011). The estimated pCO_2 by Zeebe was 12.1 µatm larger than Millero in Komuke Lagoon on average and 4.9 µatm larger in Lake Monger. At St. K7, where the leaves reached the water surface, pCO_2 was 4.8 µatm. Even at St. K1, where there was no *P. crispus*, pCO_2 was 18.7 µatm. The saturation of DO was 201% at St. K7, a higher percentage than the other stations, coincident with the lowest pCO_2 among all stations. The second lowest pCO_2 was 7.1 µatm at St. K5, with a saturation of DO of

Journal of Geophysical Research: Biogeosciences
10.1029/2022JG007032

Table 2
Total Water Depth, Leaf Length, Water Temperature, Salinity, Dissolved Oxygen, Carbonate Chemistry Parameters, pCO_2, F_a, NEP_U, NEP_L, w_e, and D_B in Komuke Lagoon

Date		8 August 2018						22 July 2019			
Station		St. B	St. D	St. H	St. J	St. K	St. M	St. F	St. J	St. P	St. Q
Total water depth (m)		0.56	1.02	1.37	1.32	1.30	1.20	1.45	1.10	1.00	1.25
Leaf length (m)		>0.56	>1.02	>1.37	>1.32	>1.30	1.20	0.50	0.70	>1.00	0.30
Water temperature (°C)	Upper	25.1	22.8	21.3	24.1	23.9	22.6	23.5	25.3	27.1	24.8
	Lower	24.0	22.4	21.2	24.1	23.7	22.3	20.8	22.7	25.7	24.2
Salinity	Upper	33.4	33.1	33.4	33.4	30.9	33.6	33.8	33.5	33.4	33.7
	Lower	33.7	33.3	33.4	33.4	33.5	34.1	33.5	33.5	33.5	33.5
DO (mg L^{-1})	Upper	9.9	9.1	7.4	7.8	7.9	7.1	9.4	13.2	17.0	10.2
	Lower	10.3	8.1	7.3	9.7	10.0	7.4	7.8	13.2	20.0	10.5
DO (%)	Upper	146	129	101	113	114	99	134	195	259	149
	Lower	149	113	100	140	143	104	107	186	297	152
DIC (μmol kg^{-1})	Upper	1,874	1,885	1,710	1,750	1,738	1,523	1,916	1,617	1,352	1,856
	Lower	1,934	1,906	1,682	1,761	1,691	1,368	1,984	1,646	1,473	1,877
TA (μmol kg^{-1})	Upper	2,229	2,198	2,073	2,212	2,201	1,995	2,222	2,215	2,149	2,224
	Lower	2,221	2,203	2,047	2,206	2,195	1,891	2,217	2,211	2,222	2,211
pCO_2 by Zeebe and Wolf-Gladrow (2001) (μatm)	Upper	299	321	208	174	158	120	353	103	40	278
	Lower	394	322	199	186	141	81	455	106	54	312
pCO_2 by Millero (2010) (μatm)	Upper	280	302	197	164	149	114	333	97	38	262
	Lower	371	303	189	176	133	78	432	100	52	294
F_a (mg-C m^{-2} day^{-1})		−89	−74	−180	−210	−226	−260	−21	−133	−162	−55
NEP_U (mg-C m^{-3} day^{-1})		322	306	274	316	314	305	52	395	1,209	60
NEP_L (mg-C m^{-3} day^{-1})		315	303	238	315	313	302	971	1,118	1,191	892
w_e (m/s)		-92.5×10^{-8}	5.23×10^{-8}	-25.1×10^{-8}	-18.4×10^{-8}	3.26×10^{-8}	5.59×10^{-9}	1.51×10^{-8}	6.09×10^{-8}	2.11×10^{-7}	1.04×10^{-9}
D_B (mg-C m^{-2} day^{-1})		89	237	169	206	182	105	468	663	1,036	270

Table 3
Total Water Depth, Leaf Length, Water Temperature, Salinity, Dissolved Oxygen, Carbonate Chemistry Parameters, pCO_2, and F_a in Lake Monger (27 November 2019)

Station		St. K1	St. K3	St. K4	St. K5	St. K7
Total water depth (m)		1.00	1.00	0.95	0.85	0.82
Leaf length (m)		0.00	0.70	0.55	>0.85	>0.82
Water temperature (℃)	Upper	24.6	25.5	25.4	25.6	25.4
	Lower	24.0	24.6	24.8	23.2	23.1
Salinity	Upper	0	0	0	0	0
	Lower	0	0	0	0	0
DO (mg L^{-1})	Upper	8.7	10.9	10.8	15.3	16.5
	Lower	8.1	12.6	11.8	16.3	18.2
DO (%)	Upper	106	133	133	189	201
	Lower	97	152	144	192	214
DIC (μmol kg^{-1})	Upper	1,504	1,453	1,454	1,365	1,334
	Lower	1,487	1,439	1,448	1,352	1,305
TA (μmol kg^{-1})	Upper	2,063	2,081	2,086	2,096	2,137
	Lower	2,074	2,077	2,080	2,101	2,135
pCO_2 by Zeebe and Wolf-Gladrow (2001) (μatm)	Upper	20.3	14.7	14.4	8.0	5.4
	Lower	17.2	13.2	13.8	6.4	3.9
pCO_2 by Millero (2010) (μatm)	Upper	11.1	8.4	8.2	5.0	3.7
	Lower	9.4	7.6	7.9	4.1	2.8
F_a (mg-C m^{-2} day^{-1})		−89	−69	−70	−70	−71
NEP_U (mg-C m^{-3} day^{-1})		0	15,688	14,916	39,662	38,782
NEP_L (mg-C m^{-3} day^{-1})		0	35,421	36,238	30,128	29,777
$\alpha_{EX} = 0.05$	w_e (m/s)	-4.49×10^{-8}[a]	2.16×10^{-7}	2.76×10^{-7}	6.57×10^{-7}	5.20×10^{-7}
	D_B (mg-C m^{-2} day^{-1})	−69[a]	1,208	958	1,448	1,329
$\alpha_{EX} = 0.10$	w_e (m/s)	-4.49×10^{-8}[a]	4.79×10^{-7}	5.99×10^{-7}	1.38×10^{-6}	1.09×10^{-6}
	D_B (mg-C m^{-2} day^{-1})	−69[a]	2,485	1,987	2,966	2,730

[a]The conceptual DIC model is not applicable.

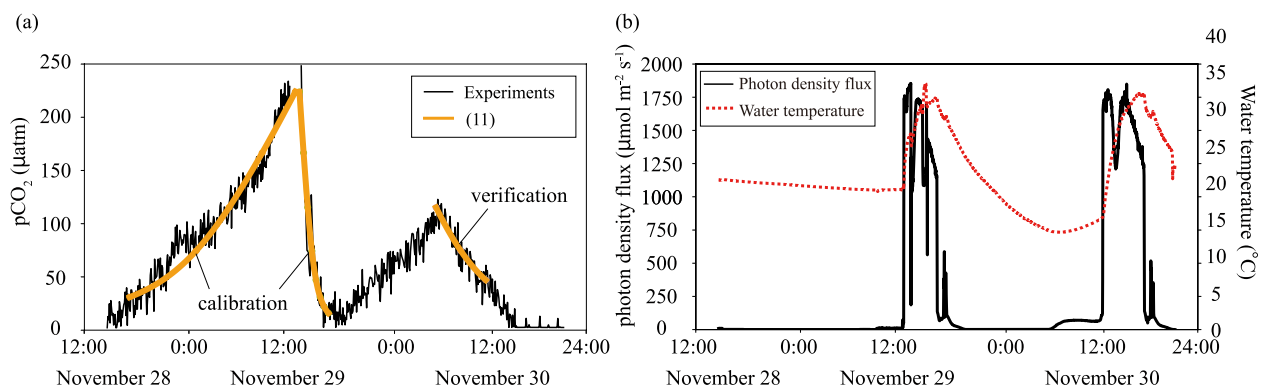

Figure 6. Laboratory experiment results assessing dissolved inorganic carbon (DIC) response of *P. crispus*. (a) pCO_2. Black and orange lines show measured and estimated pCO_2. (b) Photon flux density (black solid lines) and water temperature (red dotted lines). Productivity estimation of *P. crispus* was computed using these data by Equation 11.

189%. Therefore, we conjecture that SAV plays a significant role in reducing pCO_2 across the entire basin of Lake Monger, a freshwater lake, even though SAVs existed patchwise, suggesting that the horizontal exchange coefficient should be less than 1.0. Furthermore, it is expected that the horizontal flux of DIC at St. K1 is too large to be negligible, and the conceptual DIC model is not applicable at St. K1 because NEP is too low.

Note that the spatial density of *Z. marina* was about 25 shoots m^{-2} in Komuke Lagoon, and the spatial density of *P. crispus* was about 2,000 shoots m^{-2} in Lake Monger. The spatial density of SAVs was measured by using the underwater camera at several locations. The leaf dry weight and carbon weight were about 70 g m^{-2} m^{-1} and 20 g-C m^{-2} m^{-1} in Komuke Lagoon. Also, the leaf dry weight and carbon weight were about 547 g m^{-2} m^{-1} and 213 g-C m^{-2} m^{-1} in Lake Monger. The dry weight was measured after heating by an electric oven at 105°C for 24 hr.

3.2. Estimation of Coefficients of the DIC Equation in Lake Monger

Photon density flux was negligible from the sunset at 6:00 p.m. on the 28 to 1:00 p.m. on the 29 November in 2019, increasing pCO_2 up to about 230 µatm due to the respiration effect of *P. crispus* (Figure 6). Then, pCO_2 decreased rapidly from 1:00 p.m. to sunset at 6:00 p.m. A similar change in pCO_2 occurred from 6:00 a.m. to 1:00 p.m. on the 30. The different decrease gradients of pCO_2 between the 29 and 30 were caused by the water temperature differences. The water temperature on the 29 increased from 20°C to 35°C for 2 hr. However, it took 6 hr for the water temperature to increase from 17°C to 35°C on the 30.

Since TA was confirmed not to vary significantly among the water samples, 2,190 ± 20 µmol kg^{-1}, TA in the experimental tank was assumed to be 2,200 µmol kg^{-1} during the laboratory experiments. The parameters of the DIC equations for 2,500 shoots m^{-2} were estimated using pCO_2 from 6:00 p.m. on the 28 to 1:00 p.m. on the 29, a period when photosynthesis activity was negligible. Values for R_A and E_{aR} were obtained by assuming that the increase in DIC from 6:00 p.m. on the 28 to 1:00 p.m. on the 29 when photosynthetic activity is negligible as indicated by Equation 13. Since the DIC estimated using the measured pCO_2 fluctuated with high frequency, R_A and E_{aR} were determined to fit the overall values (Figure 6a).

$$R_A \exp\left(-\frac{E_{aR}}{T_w R}\right) = \frac{d}{dt}(\mathrm{DIC}) \tag{13}$$

The parameters for respiration were obtained as $R_A = 3 \times 10^{23}$ µmol kg^{-1} hr^{-1} and $E_{aR} = 2.04 \times 10^{-19}$ m^2 kg s^{-2} (Table 1). And then, the parameters for photosynthesis, α_ψ, were obtained by Equation 14 using R_A and E_{aR}, and the photon flux density from 1:00 p.m. to 6:00 p.m. on the 29. Since P_ψ is an unknown parameter in Equation 14, we estimated P_{coef} and E_{aP} by giving many different values of (α_ψ / P_ψ) to obtain the best fit with the laboratory experiments by trial and error. Lastly, P_ψ is obtained from Equation 15, which also gives α_ψ from (α_ψ / P_ψ).

$$P_{coef} \exp\left(-\frac{E_{aP}}{T_w R}\right) = \left[R_A \exp\left(-\frac{E_{aR}}{T_w R}\right) - \frac{d}{dt}(\mathrm{DIC})\right] / \tanh\left(\frac{\alpha_\psi I}{P_\psi}\right) \tag{14}$$

$$P_{coef} = P_\psi R_P, \text{ and } R_P = \exp\left[\frac{E_{aP}}{(273+20)R}\right] \tag{15}$$

The parameters for photosynthesis were obtained as $P_\psi = 87.7$ µmol kg^{-1} hr^{-1}, $R_P = 2.28 \times 10^{18}$, $\alpha_\psi = 87.7/90$ m^2 s kg^{-1} hr^{-1}, and $E_{aP} = 1.71 \times 10^{-19}$ m^2 kg s^{-2} (Table 1). To verify the parameters, we applied the developed DIC equation to reproduce pCO_2 from 6:00 a.m. to 0:00 p.m. on the 29, showing the high applicability of the DIC equation. Note that the optimal photon density flux was 90 µmol m^{-2} s^{-1} in Lake Monger and 200 µmol m^{-2} s^{-1} in Komuke Lagoon, indicating *P. crispus* makes a greater contribution to photon density flux than *Z. marina*.

3.3. Estimation of DIC Flux From the Bottom Sediment Using the Steady-State Two-Layer DIC Model Considering SAV

To obtain DIC flux from the sediment, we first obtained the entrainment velocity (w_e) from Equation 7 and then calculated the DIC flux from the sediment from Equation 8 because these two parameters from sediments in

Equations 7 and 8 were unknown values. The extinction coefficient was given by considering the field observations, ranging from 1.0 to 2.5 m^{-1}, to apply the conceptual DIC model to estimate DIC flux from the bottom sediment in Komuke Lagoon (Table 2). In 2018, since the leaves reached the water surface at all stations and the average wind speed was more than 5.0 m s^{-1}, net ecosystem production was almost the same in the upper and lower layers at all stations. DIC flux from the bottom sediment at St. B was the smallest, and the largest flux was at St. J. The total water depth at St. B was the smallest, which may suggest that organic matter is easily resuspended and accumulates less than in deeper areas. Therefore, DIC flux from the bottom sediment at St. B might be the smallest among all stations.

In Lake Monger, because the DIC flux from the bottom sediment should be positive, we found that the conceptual DIC model cannot be applied to the station with no SAV at St. K1, as mentioned in Section 3.1 (Table 3). The NEP in the upper layer at St. K5 and St. K7, where *P. crispus* reached the water surface, was the largest at 40,108–38,781 mg-C m^{-3} day^{-1}. Since *P. crispus* existed patchwise, the horizontal exchange coefficients were applied based on the patch are in Lake Monger, $\alpha_{EX} = 0.05$ and $\alpha_{EX} = 0.10$. The SAV abundance ratio along the field observation line from St. K1 to St. K7 was 20%–30%, respectively, suggesting that the occupancy of SAVs in Lake Monger was about 5% (=0.2^2) to 10% (=0.3^2). The DIC flux from the bottom sediment was the largest at St. K5 and St. K7, at 1,329–1,448 mg-C m^{-2} day^{-1} and 2,730–2,966 mg-C m^{-2} day^{-1}, where the leaf ratio to the depth was 1.0. In contrast, the levels of DIC flux from the bottom sediment at St. K3 and St. K4 were 958–1,208 mg-C m^{-2} day^{-1} and 1,987–2,485 mg-C m^{-2} day^{-1}, with ratios of leaf length to water depth of 0.7 m/1.0 m and 0.55 m/0.95 m, respectively. Therefore, the smaller the ratio of leaf length to total water depth, the less the DIC flux from the bottom sediment, which is similar to the relation between the ratio and DIC flux at Komuke Lagoon.

3.4. Application of the SiDIC Model

Among 15 station data sets in Komuke Lagoon and Lake Monger, we attempted to analyze the conditions in which stratification occurred clearly. If there is no stratification due to strong wind or no SAVs, it is easy to predict DIC and does not need to conduct numerical simulations. Therefore, since we aim to investigate the photosynthesis effect on carbon dioxide using numerical simulations, we picked up the stations where the SAVs existed with obvious stratifications. The vertical water temperature profiles agreed well with the field observations at all stations using the SiDIC model (Figure 7). Numerical simulations showed that the stratification at St. P, where the leaves reached the water surface, was weaker than that at St. J, which was similar to the conclusion based on the field observations. Also, the water temperature profile agreed well with the field observations under the shortest leaf condition of St. Q. Moreover, the computed DIC agreed well with the water sample values (Figure 7), suggesting the significance of leaf length for the process of stratification and DIC even when the external forces, such as meteorological conditions, are the same. Note that $\alpha_{EX} = 0.05$ was used at St. K5 in Lake Monger.

Numerical simulation results regarding the hourly change in DIC with a total water depth of 1.5 m showed the significant fluctuation of DIC and water temperature at the water surface between the daytime and nighttime. We define the difference between the maximum and minimum DIC as DIC_d. All cases indicated the increase in DIC_d with increasing leaf length (Figure 8). In cases where the leaf length was 0.5 m, the higher wind speed increased DIC_d more, excluding the density condition of the smallest submerged aquatic plants. In cases where the leaf length was 1.0 m, the mixing depth increased with increasing wind speed, resulting in an enhancement of photosynthesis in the mixing depth and an increase in DIC_d (Figure 8). To investigate the effect of stratification on carbon capture, we computed the Brunt-Väisälä frequencies. The mean Brunt-Väisälä frequencies were 12.0×10^{-5}, 9.3×10^{-5}, and 7.2×10^{-5} s^{-1} for wind speeds of 2, 4, and 6 m s^{-1} under 100 shoots m^{-2} conditions, meaning that stronger wind enhanced vertical mixing, increasing the mixing depth above SAV. Note that a similar tendency was confirmed under the other SAV density conditions. In contrast to the cases with 1.0 m leaf length, DIC_d was not linked with wind speed in the cases with 1.5 m leaf length. In the cases with 1.5 m leaf length, when the density of SAV was 100 shoots m^{-2} (10 cm spatial interval), DIC_d was the maximum at 150 μmol kg^{-1}. DIC_d was significantly correlated with the density of the SAV in the cases with 1.5 m leaf length ($r^2 = 0.9995$, p value = 0.7E−12).

To clarify the fluctuations of pCO_2 due to hourly DIC changes, we gave three different maximum pCO_2, 300, 400, and 500 μatm when the maximum DIC occurred (Figure 9). The change in pCO_2 was the larger when the pCO_2 was 500 μatm, demonstrating that the smaller the TA values, the larger the pCO_2 varies. When the density of SAV was 100 shoots m^{-2}, pCO_2 decreased to a minimum value of about 78 μatm (Figure 9c). In cases with an SAV

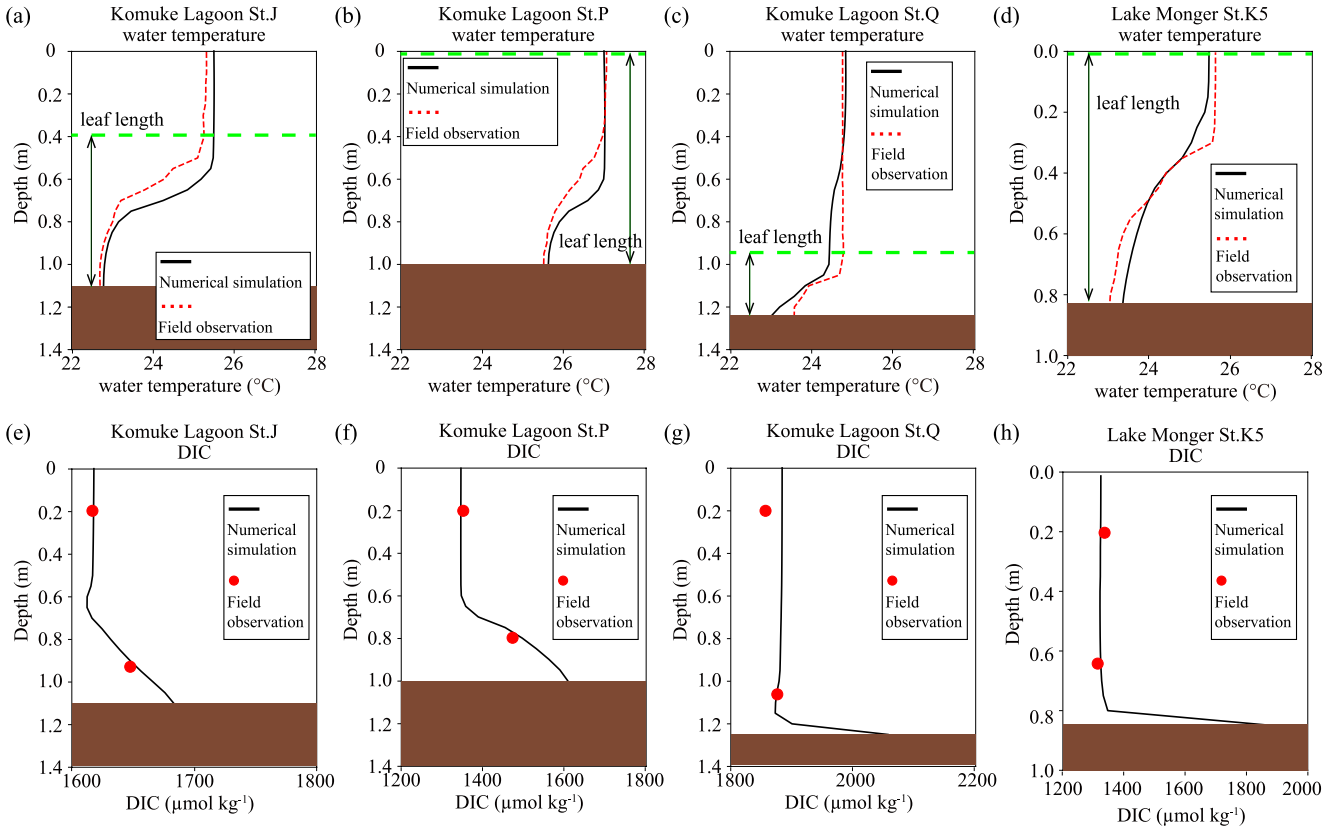

Figure 7. Numerical simulations and field observations in Komuke Lagoon on 22 July in 2019 and Lake Monger on 27 November in 2019. Green broken lines show the leaf top of submerged aquatic vegetations (SAVs). Water temperature in Komuke Lagoon at (a) St. J, (b) St. P, and (c) St. Q. Dissolved inorganic carbon (DIC) in Komuke Lagoon at (e) St. J, (f) St. P, and (g) St. Q. (d) Water temperature in Lake Monger at St. K5. (h) DIC in Lake Monger at St. K5.

density of 11 shoots m^{-2} and a leaf length of 0.5 m, the fluctuation was at a minimum of about 30 µatm. However, the other cases showed a fluctuation of more than 60 µatm, suggesting the importance of considering an hourly change in DIC. In general, the density of *Z. marina* is more than 25 shoots m^{-2} (20 cm spatial interval), and the leaf length and the total water depth ratio is more than 0.5 (e.g., Dennison & Alberte, 1985). Consequently, our study may suggest that the hourly change in DIC affects carbon dioxide flux estimation significantly. Field observation is usually conducted during the daytime, and such daytime observation may overestimate carbon capture if the fluctuation of pCO_2 is neglected. Note that the larger the pCO_2 during nighttime, the larger the pCO_2 decreases during daytime.

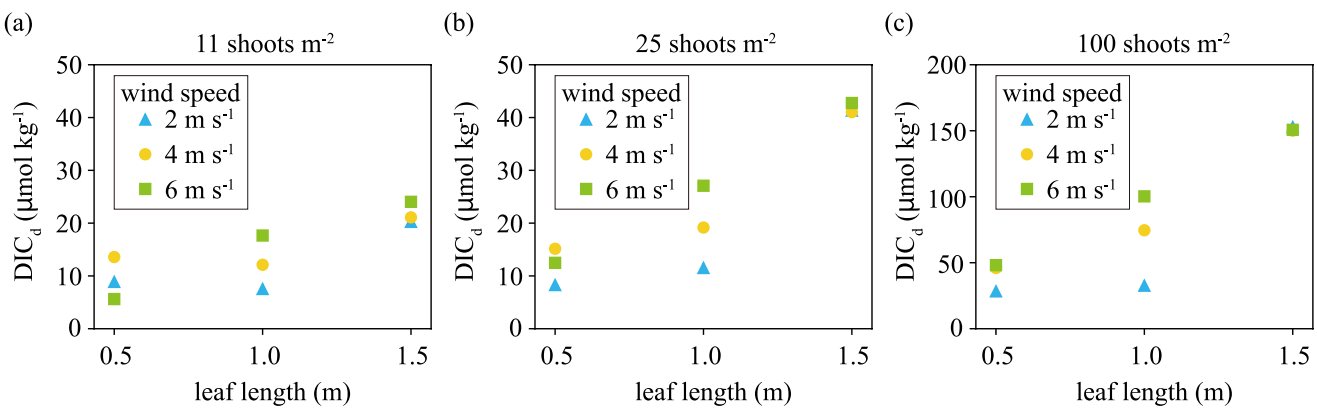

Figure 8. Daily change in dissolved inorganic carbon (DIC), difference between the maximum and minimum DIC (DIC_d). Three different wind speeds are given, 2, 4, and 6 m s^{-1}. Density of submerged aquatic vegetation (SAV) is (a) 11 shoots m^{-2}, (b) 25 shoots m^{-2}, and (c) 100 shoots m^{-2}.

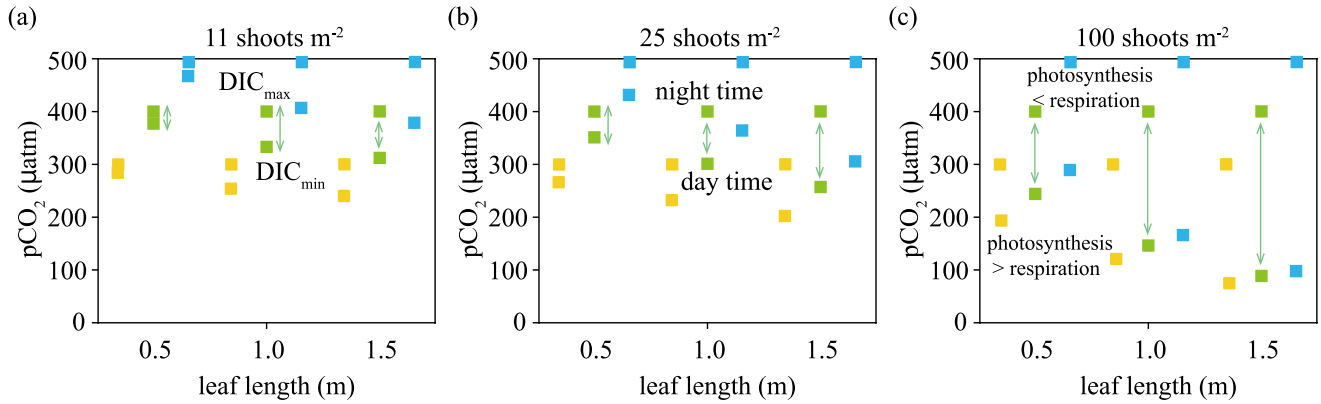

Figure 9. Maximum and minimum pCO_2 in a day. Wind speed is 6 m s^{-1}. Blue, green, and yellow squares indicate the maximum pCO_2 of 300, 400, and 500 µatm when the maximum dissolved inorganic carbon (DIC) occurred. Density of submerged aquatic vegetation (SAV) is (a) 11 shoots m^{-2}, (b) 25 shoots m^{-2}, and (c) 100 shoots m^{-2}.

4. Discussion

The spatial density of *P. crispus* was about 2,000 shoots m^{-2} in Lake Monger, and the spatial density of *Z. marina* was about 25 shoots m^{-2} in Komuke Lagoon, respectively. Noting that the dry weights for a single shoot were 0.27 and 3.67 g m^{-1} in Lake Monger and Komuke Lagoon, respectively, the increase rate of DIC for a single shoot at 20°C due to respiration in Komuke Lagoon was 2.65 (=0.0500 µmol kg^{-1} hr^{-1} $shoot^{-1}$/0.0188 µmol kg^{-1} hr^{-1} $shoot^{-1}$) times greater than that in Lake Monger due to respiration. The reduction rate of DIC for a single shoot at 20°C due to photosynthesis with a photon density flux of 1,000 µmol m^{-2} s^{-1} in Komuke Lagoon was 4.41 (=0.19 3 µmol kg^{-1} hr^{-1} $shoot^{-1}$/0.0438 µmol kg^{-1} hr^{-1} $shoot^{-1}$) times that reported for Lake Monger. Therefore, the dry weight is one of the significant factors controlling respiration and photosynthesis due to SAVs (Lee et al., 2007). Note that the effect of the attached organisms on leaves is negligibly small on the partial pressure of carbon dioxide in Komuke Lagoon and Lake Monger but not negligible in some other lakes and lagoons. Therefore, epiphytic organisms' effect on carbon absorption needs to be investigated in future studies.

In Lake Monger, St. K1 and St. K5 were chosen to examine the influence of SAV on stratification (Figure 5 and Table 3). The ratios of the *P. crispus* leaf length to the total water depth were 0.0 m/1.0 m and 0.85 m/0.85 m at St. K1 and St. K5. A slight water temperature pycnocline existed at 0.5 m from the bottom at St. K1, even though there was no *P. crispus* because of the weak wind strength of 2.0 m s^{-1}. DO was not almost consumed, suggesting that there was no influence of phytoplankton. Chl. *a* was about 3.0–5.0 µg L^{-1}. In contrast, an apparent decrease in water temperature appeared at 0.5 m from the bottom at St. K5, where the submerged aquatic plants reached the water surface. DO was about 200% (more than 15 mg L^{-1}) at St. K5, which might have been due to the photosynthesis of *P. crispus*, and DO just below the pycnocline was at the maximum due to the suppression of vertical DO flux between the upper and lower layers. The value of the saturated DO was 9 mg L^{-1}. However, the closer to the bottom, the lower the DO at St. K5. Valis et al. (2017a, 2017b) found that DO is likely to decrease in Lake Monger due to the consumption of DO by the accumulated organic matter at the lake bottom. Vilas, Adams, et al. (2017) revealed that *P. crispus* grew luxuriantly in summer, and the residence time of water inside submerged aquatic plants became longer, enhancing the occurrence of anoxia at the center of a *P. crispus* meadow and resulting in the occurrence of a ring-shaped pattern.

In 2019 at St. P of Komuke Lagoon, where the leaves reached the water surface, NEP was the largest in the upper and lower layers (Table 2). The smaller the ratio of the leaf length to the total water depth, the lower the NEP in the upper layer. The ratios were 0.7 m/1.1 m, 1.1 m/1.0 m, and 0.3 m/1.25 m at St. J, St. P, and St. Q, where the NEPs in the upper layer were 395, 1,209, and 60 mg-C m^{-3} day^{-1}, respectively. DIC flux from the bottom sediment at St. P was the largest at 1,036 mg-C m^{-2} day^{-1}. Because the smallest DIC flux was 270 mg-C m^{-2} day^{-1} at St. Q, suggesting the shorter the leaf length, the smaller the DIC flux from the bottom sediment, the exuberance of *Z. marina* may enhance the accumulation of organic matter at the bottom, resulting in the observe increase in DIC flux from the bottom sediment (Adams et al., 2016). Note that since Chl. *a* was about 2.0–6.0 µg L^{-1}, phytoplankton might not affect the increase in DO, and the supersaturated DO was expected to be due to the photosynthesis of *Z. marina* (Lin et al., 2022).

A numerical simulation model, the SiDIC model, was successfully applied to reproduce the vertical profile of water temperature and DIC in Komuke Lagoon and Lake Monger. As the eelgrass population is widely distributed in Komuke Lagoon, whose spatial scale is more than a few hundred meters, it was possible to apply the SiDIC model by assuming the spatially steady state without any influence outside of the seagrass meadow. Conversely, *P. crispus* grows densely, but they existed patchwise in Lake Monger because we conducted the field observation in early summer. The spatial scale was about tens of meters, meaning the exchange of water inside and outside of *P. crispus* meadow may not be negligible. Thus, we needed to use an unknown parameter, α_{EX}, to simulate DIC, signifying the limitation of the SiDIC model application to SAV meadows. Indeed, Chen et al. (2013) revealed that the mixing layer is fully developed at a distance from the leading edge of the meadow, which is a function of mean horizontal velocity, the shear-length scale, and friction velocity, meaning that the horizontally uniform assumption is available when the horizontal scale of SAV meadows is longer than Chen's scale. Therefore, we may suggest being careful about the horizontal scale of SAV meadows when we apply the SiDIC model to investigate the vertical flux of DIC.

The durations of photon flux density have been used to evaluate the rate of eelgrass production (Dennison & Alberte, 1982, 1985). This may suggest that pCO_2 varies hourly during 1 day. Therefore, we carried out our simulation over 2 days, using the meteorological data on the 22 July 2019 at St. P to understand the fluctuation of pCO_2. The meteorological and other conditions on the second day were considered to be the same as those on the first day to obtain stable fluctuations. Water temperature at the water surface reached about 30°C during the daytime and decreased to about 27°C during the nighttime. In contrast, DIC increased to about 1,390 μmol kg^{-1} from 8:00 p.m. on the first day to 7:00 on the second day. Then, DIC decreased to about 1,340 μmol kg^{-1} at 8:00 p.m. In a case with TA of 1,572 μmol kg^{-1}, the maximum and minimum pCO_2 were 400 and 322 μatm during the nighttime and daytime, respectively, indicating the crucial hourly fluctuation of DIC and the necessity of evaluating carbon dioxide flux, including the hourly change in DIC. If the nighttime pCO_2 is more than 400 μatm, such as 500 μatm, pCO_2 decreases slightly more than 78 μatm during the daytime (Figure 9). In contrast, if the nighttime pCO_2 is 300 μatm, pCO_2 decreases slightly less than 78 μatm during the daytime, suggesting that the smaller the TA, the larger the pCO_2 varies. However, the sensitivity analysis showed that the most significant factor is the spatial density of SAV (Figure 9). The second is the leaf length ratio to total depth, and the initial TA value is a minor effect on the changes in the pCO_2 values.

On the other hand, since a topographic effect (change in water depth) has been shown to influence the photon flux density under water—as well as the spatial distribution of nutrients, the turbidity and other parameters—it is thought that physical conditions strongly contribute to the growth rate of *Z. marina* (Dennison, 1987; Dennison & Alberte, 1986). Additionally, the minimum light requirement has been investigated, revealing that there is a large variability in the minimum light requirement (Dennison et al., 1993; Koch & Beer, 1996; Olesen & Sand-Jensen, 1993). Hence, the ratio of leaf length to total water depth may be significant to estimate carbon capture due to SAV (Figure 10). The mixing depth caused by wind stress at the water surface may be one of the most significant factors, because the mixing depth is associated with the vertical flux of DIC, which varies due to respiration and photosynthesis related to carbon capture. Additionally, it is significant to estimate how much carbon dioxide is released from the accumulated SAVs at the bottom in terms of the vertical DIC flux. Therefore, it is necessary to investigate the decomposition of organic matter inside the bottom sediment and the mineralization process from dissolved organic carbon to DIC in future studies.

5. Conclusion

A conceptual DIC model was proposed using the field observations at Komuke Lake and Lake Monger, enabling us to estimate DIC flux from the bottom sediment. The density of SAV is higher in Lake Monger than in Komuke Lagoon, and thus anoxia is more likely to occur in Lake Monger, and DIC flux from the bottom sediment in Lake Monger was about twice as much as that at Komuke Lagoon. pCO_2 and NEP were lower and larger, respectively, in Lake Monger than the Komuke Lagoon, suggesting the potential significance of "freshwater blue carbon" or "freshwater carbon" when SAV is dense and dominates water quality (S. Watanabe et al., 2023). To allow system scale simulations able to meaningfully resolve feedbacks between flow and vegetation, a subgrid-scale SAV approach, GiSAV, was developed by integrating a bundle of submerged aquatic plants into one aggregated SAV element to reduce runtime costs. Using this simplification, the SiDIC model was developed and able to reveal the significant hourly fluctuation of DIC throughout the water column. When leaf length was 1.0 m with a total water

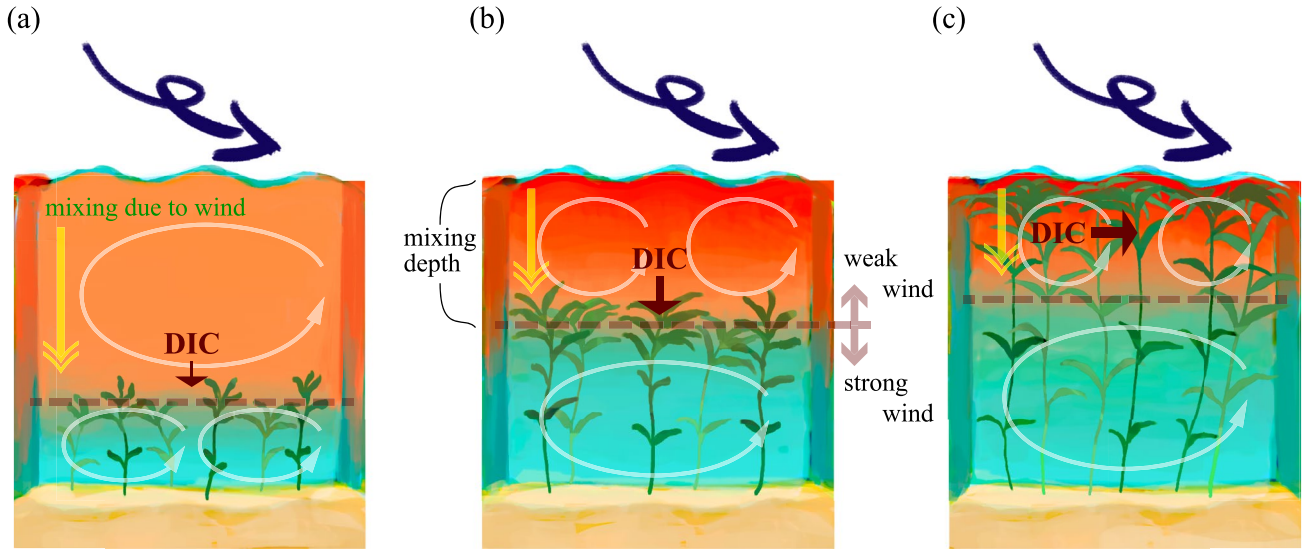

Figure 10. Effects of leaf length and wind stress on the formation of mixing depth. (a) Submerged aquatic plants exist adjacent to the lake bottom. (b) The leaves do not reach the water surface. (c) Leaf length is longer than total water depth. Illustration adapted with permission from Reina Nakayama.

depth of 1.5 m, the higher wind speed was found to increase the mixing depth determined by the mixing depth in stratification, thereby increasing DIC_d. Furthermore, the density of SAV has a strong correlation with DIC_d when leaf length is longer than the total water depth. It was revealed that pCO_2 fluctuation between daytime and nighttime is substantial in real fields. Therefore, we may recommend estimating carbon dioxide flux by conducting a continuous field observation for extended periods or by applying numerical models, such as in the SiDIC model, which enable to accurately evaluate the effect of respiration and photosynthesis on DIC when calibrated with laboratory experiments. The use of daytime observations only may lead to an underestimation of the pCO_2 and hence an overestimation of carbon capture and storage within freshwater lakes and coastal environments. Note that the SiDIC model could also be useful for investigating the pCO_2 estimation without vegetation in a stratified fluid, such as lakes and the estuary.

Conflict of Interest

The authors declare no conflicts of interest relevant to this study.

Data Availability Statement

The executable binary (windows, Mac, and Linux) of the three-dimensional hydrodynamic model, Fantom, used in this study, is available from http://www.comp.tmu.ac.jp/shintani/fantom.html. The model outputs are available from https://doi.org/10.5281/zenodo.7273833. The data sets for Nagatomo et al. (2022).

Acknowledgments
This work was supported by the Japan Society for the Promotion of Science under Grants 22H01601, 22H05726, and 18KK0119. We owe special thanks to R. Nakayama for constructing figures. M. R. H. received funding from Australian Research Council projects LP150100519 and LP200200910.

References

Abdolahpour, M., Ghisalberti, M., McMahon, K., & Lavery, P. S. (2018). The impact of flexibility on flow, turbulence, and vertical mixing in coastal canopies. *Limnology & Oceanography*, *63*(6), 2777–2792. https://doi.org/10.1002/lno.11008

Adams, P. A., Hovey, R. K., Hipsey, M. R., Bruce, L. C., Ghisalberti, M., Lowe, R. J., et al. (2016). Feedback between sediment and light for seagrass: Where is it important? *Limnology & Oceanography*, *61*(6), 1937–1955. https://doi.org/10.1002/lno.10319

Baird, M. E., Adams, M. P., Babcock, R. C., Oubelkheir, K., Mongin, M., Wild-Allen, K. A., et al. (2016). A biophysical representation of seagrass growth for application in a complex shallow-water biogeochemical model. *Ecological Modelling*, *325*, 13–27. https://doi.org/10.1016/j.ecolmodel.2015.12.011

Bauer, J. E., Cai, W., Raymond, P. A., Bianchi, T. S., Hopkinson, C. S., & Regnier, P. A. G. (2013). The changing carbon cycle of the coastal ocean. *Nature*, *504*(7478), 61–70. https://doi.org/10.1038/nature12857

Beca-Carretero, P., Olesen, B., Marba, N., & Krause-Jensen, D. (2018). Response to experimental warming in northern eelgrass populations: Comparison across a range of temperature adaptations. *Marine Ecology Progress Series*, *589*, 59–72. https://doi.org/10.3354/meps12439

Burkholz, C., Duarte, C. M., & Garcias-Bonet, N. (2019). Thermal dependence of seagrass ecosystem metabolism in the Red Sea. *Marine Ecology Progress Series*, *614*, 79–90. https://doi.org/10.3354/meps12912

Casamitjana, X., Menció, A., Quintana, X. D., Soler, D., Compte, J., Martinoy, M., & Pascual, J. (2019). Modeling the salinity fluctuations in salt marsh lagoons. *Journal of Hydrology*, *575*, 1178–1187. https://doi.org/10.1016/j.jhydrol.2019.06.018

Chen, Z., Jiang, C., & Nepf, H. (2013). Flow adjustment at the leading edge of a submerged aquatic canopy. *Water Resources Research*, *49*, 5537–5551. https://doi.org/10.1002/wrcr.20403

Dennison, W. C. (1987). Effects of light on seagrass photosynthesis, growth and depth distribution. *Aquatic Botany*, *27*(1), 15–26. https://doi.org/10.1016/0304-3770(87)90083-0

Dennison, W. C., & Alberte, R. S. (1982). Photosynthetic responses of *Zostera marina* L. (eelgrass) to in situ manipulations of light intensity. *Oecologia*, *55*(2), 137–144. https://doi.org/10.1007/BF00384478

Dennison, W. C., & Alberte, R. S. (1985). Role of daily light period in the depth distribution of *Zostera marina* (eelgrass). *Marine Ecology Progress Series*, *25*, 51–61. https://doi.org/10.3354/meps025051

Dennison, W. C., & Alberte, R. S. (1986). Photoadaptation and growth of *Zostera marina* L. (eelgrass) transplants along a depth gradient. *Journal of Experimental Marine Biology and Ecology*, *98*(3), 265–282. https://doi.org/10.1016/0022-0981(86)90217-0

Dennison, W. C., Orth, R. J., Moore, K. A., Stevenson, J. C., Carter, V., Kollar, S., et al. (1993). Assessing water quality with submersed aquatic vegetation: Habitat requirements as barometers of Chesapeake Bay health. *BioScience*, *43*(2), 86–94. https://doi.org/10.2307/1311969

Dickson, A. G. (1990). Standard potential of the reaction: AgCl(s) + 12H2(g) = Ag(s) + HCl(aq), and and the standard acidity constant of the ion HSO4− in synthetic sea water from 273.15 to 318.15 K. *The Journal of Chemical Thermodynamics*, *22*(2), 113–127. https://doi.org/10.1016/0021-9614(90)90074-Z

A. G. Dickson, C. L. Sabine, & J. R. Christian (Eds.). (2007). Guide to best practices for 622 ocean CO_2 measurements. In *PICES Special Publication 3* (p 3191, chap. 4, SOP). Retrieved from https://cdiac.ess-623dive.lbl.gov/ftp/oceans/Handbook_2007/Guide_all_in_one.pdf

Drew, E. A. (1979). Physiological aspects of primary production in seagrasses. *Aquatic Botany*, *7*, 139–150. https://doi.org/10.1016/0304-3770(79)90018-4

Ghisalberti, M., & Nepf, H. (2006). The structure of the shear layer in flows over rigid and flexible canopies. *Environmental Fluid Mechanics*, *6*(3), 277–301. https://doi.org/10.1007/s10652-006-0002-4

Ghisalberti, M., & Nepf, H. (2009). Shallow flows over a permeable medium: The hydrodynamics of submerged aquatic canopies. *Transport in Porous Media*, *78*(3), 309–326. https://doi.org/10.1007/s11242-009-9434-x

Goodman, J. L., Moore, K. A., & Dennison, W. C. (1995). Photosynthetic responses of eelgrass (*Zostera marina* L.) to light and sediment sulfide in a shallow barrier island lagoon. *Aquatic Botany*, *50*(1), 37–47. https://doi.org/10.1016/0304-3770(94)00444-Q

Hipsey, M. R., Bruce, L. C., Boon, C., Busch, B., Carey, C. C., Hamilton, D. P., et al. (2019). A General Lake Model (GLM 3.0) for linking with high-frequency sensor data from the Global Lake Ecological Observatory Network (GLEON). *Geoscientific Model Development*, *12*(1), 473–523. https://doi.org/10.5194/gmd-12-473-2019

Holmer, M., & Bondgaard, E. J. (2001). Photosynthetic and growth response of eelgrass to low oxygen and high sulfide concentrations during hypoxic events. *Aquatic Botany*, *70*(1), 29–38. https://doi.org/10.1016/S0304-3770(00)00142-X

Hu, X., & Cai, W. J. (2013). Estuarine acidification and minimum buffer zone—A conceptual 481 study. *Geophysical Research Letters*, *40*, 5176–5181. https://doi.org/10.1002/grl.51000

Imberger, J., Patterson, J., Hebbert, B., & Loh, I. (1978). Dynamics of reservoir of medium size. *Journal of the Hydraulics Division*, *104*(5), 725–743. https://doi.org/10.1061/JYCEAJ.0004997

IPCC. (2014). In Core Writing Team, R. K. Pachauri, & L. A. Meyer (Eds.), *Climate change 2014: Synthesis report. Contribution of Working Groups I, II and III to the Fifth Assessment Report of the Intergovernmental Panel on Climate Change* (p. 151). IPCC.

IPCC. (2018). In V. Masson-Delmotte, et al. (Eds.), *Global warming of 1.5°C. An IPCC Special Report on the impacts of global warming of 1.5°C above pre-industrial levels and related global greenhouse gas emission pathways, in the context of strengthening the global response to the threat of climate change, sustainable development, and efforts to eradicate poverty* (p. 616). IPCC.

IPCC. (2021). Summary for policymakers. In V. Masson-Delmotte, et al. (Eds.), *Climate change 2021: The physical science basis. Contribution of Working Group I to the Sixth Assessment Report of the Intergovernmental Panel on Climate Change* (41 pp.). IPCC.

Jähne, B., Heinz, G., & Dietrich, W. (1987). Measurement of the diffusion-coefficients of sparingly soluble gases in water. *Journal of Geophysical Research*, *92*(C10), 10767–10776. https://doi.org/10.1029/JC092iC10p10767

Jones, H. F., Özkundakci, D., McBride, C. G., Pilditch, C. A., Allan, M. G., & Hamilton, D. P. (2018). Modelling interactive effects of multiple disturbances on a coastal lake ecosystem: Implications for management. *Journal of Environmental Management*, *207*, 444–455. https://doi.org/10.1016/j.jenvman.2017.11.063

Jones, W. P., & Launder, B. E. (1972). The prediction of laminarization with a two-equation model of turbulence. *International Journal of Heat and Mass Transfer*, *15*(2), 301–314. https://doi.org/10.1016/0017-9310(72)90076-2

Karle, I., Hall, P. O. J., & Dahllöf, I. (2007). Biogeochemical response of an intact coastal sediment to organic matter input: A multivariate approach. *Marine Ecology Progress Series*, *342*, 15–25. https://doi.org/10.3354/meps342015

Koch, E. W., & Beer, S. (1996). Tides, light and the distribution of *Zostera marina* in Long Island Sound, USA. *Aquatic Botany*, *53*(1–2), 97–107. https://doi.org/10.1016/0304-3770(95)01015-7

Ladwig, R., Hanson, P. C., Dugan, H. A., Carey, C. C., Zhang, Y., Shu, L., et al. (2021). Lake thermal structure drives interannual variability in summer anoxia dynamics in a eutrophic lake over 37 years. *Hydrology and Earth System Sciences*, *25*(2), 1009–1032. https://doi.org/10.5194/hess-25-1009-2021

Lee, K. S., Park, S. R., & Kim, Y. K. (2007). Effects of irradiance, temperature, and nutrients on growth dynamics of seagrasses: A review. *Journal of Experimental Marine Biology and Ecology*, *350*(1–2), 144–175. https://doi.org/10.1016/j.jembe.2007.06.016

Lehrter, J. C., Beddick, D. L., Jr., Devereux, R., Yates, D. F., & Murrell, M. C. (2012). Sediment-water fluxes of dissolved inorganic carbon, O_2, nutrients, and N_2 from the hypoxic region of the Louisiana continental shelf. *Biogeochemistry*, *109*(1/3), 233–252. https://doi.org/10.1007/s10533-011-9623-x

Lewis, E. R., & Wallace, D. W. R. (1998). Program developed for CO_2 system calculations. Rep. oRNL/CDIAC-105.United States Department of Energy.

Lin, H. C., Chiu, C. Y., Tsai, J. W., Liu, W. C., Tada, K., & Nakayama, K. (2021). Influence of thermal stratification on seasonal net ecosystem production and dissolved inorganic carbon in a shallow subtropical lake. *Journal of Geophysical Research: Biogeosciences*, *126*, e2020JG005907. https://doi.org/10.1029/2020JG005907

Lin, H. C., Tsai, J. W., Tada, K., Matsumoto, H., Chiu, C. Y., & Nakayama, K. (2022). The impacts of the hydraulic retention effect and typhoon disturbance on the carbon flux in shallow subtropical mountain lakes. *Science of The Total Environment*, *803*(10), 150044. https://doi.org/10.1016/j.scitotenv.2021.150044

Marsh, J. A., Jr., Dennison, W. C., & Alberte, R. S. (1986). Effects of temperature on photosynthesis and respiration in eelgrass (*Zostera marina* L.). *Journal of Experimental Marine Biology and Ecology*, *101*(3), 257–267. https://doi.org/10.1016/0022-0981(86)90267-4

Matsumoto, H., Nakayama, K., Komai, K., Tada, K., Sadaki, D., Watanabe, K., et al. (2020). Development of a model for estimating of vertical distribution of dissolved inorganic carbon due to eelgrass in a stratified fluid (in Japanese with English abstract). *Journal of Japan Society of Civil Engineers Series B3 (Ocean Engineering)*, *76*(2), I_869–I_874. https://doi.org/10.2208/jscejoe.76.2_I_869

Millero, F. (2010). Carbonate constants for estuarine waters. *Marine and Freshwater Research*, *61*(2), 139–142. https://doi.org/10.1071/mf09254

Nakayama, K., Komai, K., Tada, K., Lin, H. C., Yajima, K., Yano, S., et al. (2020). Modelling dissolved inorganic carbon considering submerged aquatic vegetation. *Ecological Modelling*, *431*, 109188. https://doi.org/10.1016/j.ecolmodel.2020.109188

Nakayama, K., Nakagawa, Y., Nakanishi, Y., Kuwae, T., Watanabe, K., Moki, H., et al. (2020). Integration of submerged aquatic vegetation motion within hydrodynamic models. *Water Resources Research*, *56*, e2020WR027369. https://doi.org/10.1029/2020WR027369

Nakayama, K., Nguyen, H. D., Shintani, T., & Komai, K. (2016). Reversal of secondary circulations in a sharp channel bend. *Coastal Engineering Journal*, *58*(2), 1650002-1–1650002-23. https://doi.org/10.1142/S0578563416500029

Nakayama, K., Sato, T., Tani, K., Boegman, L., & Fujita, I. (2020). Breaking of internal Kelvin wave shoaling on a slope. *Journal of Geophysical Research: Oceans*, *125*, e2020JC016120. https://doi.org/10.1029/2020JC016120

Nakayama, K., Shintani, T., Shimizu, K., Okada, T., Hinata, H., & Komai, K. (2014). Horizontal and residual circulations driven by wind stress curl in Tokyo Bay. *Journal of Geophysical Research: Oceans*, *119*, 1977–1992. https://doi.org/10.1002/2013JC009396

Nakayama, K., Sivapalan, M., Sato, C., & Furukawa, K. (2010). Stochastic characterization of the onset of and recovery from hypoxia in Tokyo Bay, Japan: Derived distribution analysis based on "strong wind" events. *Water Resources Research*, *46*, W12532. https://doi.org/10.1029/2009WR008900

Nellemann, C., Corcoran, E., Duarte, C. M., Valdes, L., DeYoung, C., Fonseca, L., & Grimsditch, G. (2009). *Blue carbon. A Rapid response assessment*. United Nations Environmental Programme, GRID-Arendal.

Nepf, H. M. (2012). Flow and transport in regions with aquatic vegetation. *Annual Review of Fluid Mechanics*, *44*(1), 123–142. https://doi.org/10.1146/annurev-fluid-120710-101048

Okely, P., & Imberger, J. (2007). Horizontal transport induced by upwelling in a canyon-shaped reservoir. *Hydrobiologia*, *586*(1), 343–355. https://doi.org/10.1007/s10750-007-0706-6

Olesen, B., & Sand-Jensen, K. (1993). Seasonal acclimatization of eelgrass *Zostera marina* growth to light. *Marine Ecology Progress Series*, *94*, 91–99. https://doi.org/10.3354/meps094091

Simpson, E., Ianson, D., & Kohfeld, K. E. (2022). Using end-member models to estimate seasonal carbonate chemistry and acidification sensitivity in temperate estuaries. *Geophysical Research Letters*, *49*, e2021GL095579. https://doi.org/10.1029/2021GL095579

Staehr, P. A., & Borum, J. (2011). Seasonal acclimation in metabolism reduces light requirements of eelgrass (*Zostera marina*). *Journal of Experimental Marine Biology and Ecology*, *407*(2), 139–146. https://doi.org/10.1016/j.jembe.2011.05.031

Touchette, B. W. (1999). *Physiological and developmental responses of eelgrass (Zostera marina* L.) to increases in water-column nitrate and temperature (Ph.D. dissertation). North Carolina State University.

Trolle, D., Elliott, J. A., Mooij, W. M., Janse, J. H., Bolding, K., Hamilton, D. P., & Jeppesen, E. (2014). Advancing projections of phytoplankton responses to climate change through ensemble modelling. *Environmental Modelling & Software*, *61*, 371–379. https://doi.org/10.1016/j.envsoft.2014.01.032

Trolle, D., Hamilton, D. P., Hipsey, M. R., Bolding, K., Bruggeman, J., Mooij, W. M., et al. (2012). A community-based framework for aquatic ecosystem models. *Hydrobiologia*, *683*(1), 25–34. https://doi.org/10.1007/s10750-011-0957-0

Umlauf, L., & Burchard, H. (2003). A generic length-scale equation for geophysical turbulence models. *Journal of Marine Research*, *61*(2), 235–265. https://doi.org/10.1357/002224003322005087

van Heuven, S., Pierrot, D., Rae, J. W. B., Lewis, E. R., & Wallace, D. W. R. (2011). MATLAB program developed for CO_2 system calculations. ORNL/CDIAC-105b. Carbon Dioxide Information Analysis Center, Oak Ridge National Laboratory, U.S. Department of Energy. https://doi.org/10.3334/CDIAC/otg.CO2SYS_MATLAB_v1.1

Vilas, M. P., Adams, M. P., Oldhamc, C. E., Martid, C. L., & Hipsey, M. R. (2017). Fragment dispersal and plant-induced dieback explain irregular ring-shaped pattern formation in a clonal submerged macrophyte. *Ecological Modelling*, *363*, 111–121. https://doi.org/10.1016/j.ecolmodel.2017.09.001

Vilas, M. P., Marti, C. L., Adams, M. P., Oldham, C. E., & Hipsey, M. R. (2017). Invasive macrophytes control the spatial and temporal patterns of temperature and dissolved oxygen in a shallow lake: A proposed feedback mechanism of macrophyte loss. *Frontiers of Plant Science*, *8*, 1–14. https://doi.org/10.3389/fpls.2017.02097

Wannikhof, R. (1992). Relationship between wind speed and gas exchange over the ocean. *Journal of Geophysical Research*, *97*(C5), 7373–7382. https://doi.org/10.1029/92JC00188

Watanabe, K., & Kuwae, T. (2021). An unintended ecological benefit from human intervention: The enhancement of carbon storage in seagrass meadows. *Journal of Applied Ecology*, *58*(11), 2441–2452. https://doi.org/10.1111/1365-2664.13977

Watanabe, S., Maruya, Y., Yano, S., & Nakayama, K. (2023). Perceptions of practitioners on the importance and achievement of research and social implementation activities on blue carbon. *Frontiers in Marine Science*, *9*, 1036248. https://doi.org/10.3389/fmars.2022.1036248

Weiss, R. F. (1974). Carbon dioxide in water and seawater: The solubility of a non-ideal gas. *Marine Chemistry*, *2*(C3), 203–215. https://doi.org/10.1016/0304-4203(74)90015-2

Weitzman, J. S., Zeller, R. B., Thomas, F. I. M., & Koseff, J. R. (2015). The attenuation of current- and wave-driven flow within submerged multispecific vegetative canopies. *Limnology & Oceanography*, *60*(6), 1855–1874. https://doi.org/10.1002/lno.10121

Yeates, P. S., Gomez-Giraldo, A., & Imberger, J. (2013). Observed relationships between microstructure patches and the gradient Richardson number in a thermally stratified lake. *Environmental Fluid Mechanics*, *13*(3), 205–226. https://doi.org/10.1007/s10652-013-9269-4

Zeebe, R. E., & Wolf-Gladrow, D. (2001). *CO_2 in seawater: Equilibrium, kinetics, isotopes* (pp. 1–83). Elsevier.

Zeller, R. B., Weitzman, J. S., Abbett, M. E., Zarama, F. J., Fringer, O. B., & Koseff, J. R. (2014). Improved parameterization of seagrass blade dynamics and wave attenuation based on numerical and laboratory experiments. *Limnology & Oceanography*, *59*(1), 251–266. https://doi.org/10.4319/lo.2014.59.1.0251

Zhang, X., Wang, K., Frassl, M. A., & Boehrer, B. (2020). Reconstructing six decades of surface temperatures at a shallow lake. *Water*, *12*(2), 405. https://doi.org/10.3390/w12020405

Zhou, W., Imberger, J., & Marti, C. L. (2021). A new pseudo three-dimensional hydrodynamic model with Lagrangian vertical mixing and Eulerian horizontal mass exchange. *Environmental Modelling & Software*, *143*, 105099. https://doi.org/10.1016/j.envsoft.2021.105099

Zimmerman, R. C., Kohrs, D. G., Steller, D. L., & Alberte, R. S. (1997). Impacts of CO_2 enrichment on productivity and light requirements of eelgrass. *Plant Physiology*, *115*(2), 599–607. https://doi.org/10.1104/pp.115.2.599

Zimmerman, R. C., Reguzzoni, J. L., & Alberte, R. S. (1995). Eelgrass (*Zostera marina* L.) transplants in san Francisco Bay: Role of light availability on metabolism, growth and survival. *Aquatic Botany*, *51*(1–2), 67–86. https://doi.org/10.1016/0304-3770(95)00472-C